



**JULES: carbon fluxes  
and vegetation**

D. B. Clark et al.

This discussion paper is/has been under review for the journal Geoscientific Model Development (GMD). Please refer to the corresponding final paper in GMD if available.

# The Joint UK Land Environment Simulator (JULES), Model description – Part 2: Carbon fluxes and vegetation

D. B. Clark<sup>1</sup>, L. M. Mercado<sup>1</sup>, S. Sitch<sup>2</sup>, C. D. Jones<sup>3</sup>, N. Gedney<sup>4</sup>, M. J. Best<sup>3</sup>, M. Pryor<sup>4</sup>, G. G. Rooney<sup>3</sup>, R. L. H. Essery<sup>5</sup>, E. Blyth<sup>1</sup>, O. Boucher<sup>3</sup>, R. J. Harding<sup>1</sup>, and P. M. Cox<sup>6</sup>

<sup>1</sup>Centre for Ecology and Hydrology, Wallingford, OX10 8BB, UK

<sup>2</sup>School of Geography, University of Leeds, Leeds LS2 9JT, UK

<sup>3</sup>Met Office Hadley Centre, Exeter, EX1 3PB, UK

<sup>4</sup>Met Office, Joint Centre for Hydro-Meteorological research, Wallingford, OX10 8BB, UK

<sup>5</sup>School of GeoSciences, University of Edinburgh, EH9 3JW, Edinburgh, UK

<sup>6</sup>College of Engineering, Mathematics and Physical Sciences, University of Exeter, Exeter, EX4 4QF, UK

Received: 2 March 2011 – Accepted: 4 March 2011 – Published: 24 March 2011

Correspondence to: D. B. Clark (dbcl@ceh.ac.uk)

Published by Copernicus Publications on behalf of the European Geosciences Union.

Title Page

Abstract

Introduction

Conclusions

References

Tables

Figures

◀

▶

◀

▶

Back

Close

Full Screen / Esc

Printer-friendly Version

Interactive Discussion



## Abstract

The Joint UK Land Environment Simulator (JULES) is a process-based model that simulates the fluxes of carbon, water, energy and momentum between the land surface and the atmosphere. Past studies with JULES have demonstrated the important role of the land surface in the Earth System. Different versions of JULES have been employed to quantify the effects on the land carbon sink of separately changing atmospheric aerosols and tropospheric ozone, and the response of methane emissions from wetlands to climate change. There was a need to consolidate these and other advances into a single model code so as to be able to study interactions in a consistent manner. This paper describes the consolidation of these advances into the modelling of carbon fluxes and stores, in the vegetation and soil, in version 2.2 of JULES. Features include a multi-layer canopy scheme for light interception, including a sunfleck penetration scheme, a coupled scheme of leaf photosynthesis and stomatal conductance, representation of the effects of ozone on leaf physiology, and a description of methane emissions from wetlands. JULES represents the carbon allocation, growth and population dynamics of five plant functional types. The turnover of carbon from living plant tissues is fed into a 4-pool soil carbon model. The process-based descriptions of key ecological processes and trace gas fluxes in JULES mean that this community model is well-suited for use in carbon cycle, climate change and impacts studies, either in standalone mode or as the land component of a coupled Earth system model.

## 1 Introduction

Terrestrial ecosystems play an important role in land surface energy and trace gas exchange with the atmosphere. They currently absorb almost one third of the anthropogenic carbon dioxide emissions (Prentice et al., 2001; Le Quéré et al., 2009), although the locations and mechanisms for these terrestrial carbon sinks are debated and uncertain (Ciais et al., 1995; McGuire et al., 2001; Stephens et al., 2007; Phillips

**GMDD**

4, 641–688, 2011

## JULES: carbon fluxes and vegetation

D. B. Clark et al.

[Title Page](#)

[Abstract](#)

[Introduction](#)

[Conclusions](#)

[References](#)

[Tables](#)

[Figures](#)

[⏪](#)

[⏩](#)

[◀](#)

[▶](#)

[Back](#)

[Close](#)

[Full Screen / Esc](#)

[Printer-friendly Version](#)

[Interactive Discussion](#)



et al., 2009). Furthermore, land-atmosphere exchange of non-CO<sub>2</sub> greenhouse gases, such as CH<sub>4</sub>, O<sub>3</sub>, and N<sub>2</sub>O, affect atmospheric chemistry and climate (Arneth et al., 2010). Vegetation and soils also exert a strong control on the surface energy balance and the physical state of the atmosphere. Anthropogenic climate change has been projected to radically alter the structure and function of terrestrial ecosystems (Cramer et al., 2001; Sitch et al., 2008). Future shifts in vegetation, such as a northward migration of the boreal forest into tundra, are likely to impact the climate via both biogeophysical and biogeochemical feedbacks. This spurred the development of Dynamic Global Vegetation Models (DGVMs; Cox, 2001; Sitch et al., 2003; Prentice et al., 2007) which describe the structure and function of the major global terrestrial ecosystems.

Advances in recent years have seen the inclusion in land surface models of first a carbon cycle (Cox et al., 2000) and a nitrogen cycle (Thornton et al., 2007; Sokolov et al., 2008). Using the TRIFFID DGVM coupled to a General Circulation Model (HadCM3LC), Cox et al. (2000) were the first to show the possibility of a positive climate-land carbon cycle feedback, through the counteracting effects of climate and atmospheric CO<sub>2</sub> on ecosystem function. A reduction in terrestrial carbon in response to climate change, leads to higher atmospheric CO<sub>2</sub> levels, and thus accelerated climate change. This has major policy implications for climate change mitigation (Jones et al., 2006). Friedlingstein et al. (2006) extended this work using 11 coupled climate-carbon cycle models. All models simulated a positive land carbon cycle feedback but of widely varying strengths and there was little consensus among models on the underlying mechanisms.

The land surface scheme used by Cox et al. (2000) was the Met Office Surface Exchange Scheme (MOSES; Cox et al., 1999; Essery et al., 2003). The representation of plant and soil processes in this model, and the implications for the modelled carbon cycle, have been the subject of several subsequent studies. In Cox et al. (2000) the positive feedback is attributed to enhanced soil decomposition in mid-latitudes with warming, and drought induced forest dieback across Amazonia (Betts et al., 2004; Cox et al., 2004). Subsequent studies investigated the structural uncertainty in future projections

**JULES: carbon fluxes  
and vegetation**

D. B. Clark et al.

[Title Page](#)[Abstract](#)[Introduction](#)[Conclusions](#)[References](#)[Tables](#)[Figures](#)[◀](#)[▶](#)[◀](#)[▶](#)[Back](#)[Close](#)[Full Screen / Esc](#)[Printer-friendly Version](#)[Interactive Discussion](#)

**JULES: carbon fluxes  
and vegetation**

D. B. Clark et al.

[Title Page](#)[Abstract](#)[Introduction](#)[Conclusions](#)[References](#)[Tables](#)[Figures](#)[◀](#)[▶](#)[◀](#)[▶](#)[Back](#)[Close](#)[Full Screen / Esc](#)[Printer-friendly Version](#)[Interactive Discussion](#)

associated with the soil carbon representation (Jones et al., 2005), the role of tropical ecosystems in the control of atmospheric CO<sub>2</sub> on the interannual timescales (Jones et al., 2003), and evaluated the coupled model against atmospheric data, proposing a prototype benchmarking methodology for coupled climate-carbon cycle models (Cadule et al., 2010). Jones et al. (2005) replaced the one-pool soil decomposition model with the more elaborate 4-pool model of RothC (Jenkinson, 1990; Coleman and Jenkinson, 1999) and concluded that the projection of a positive feedback between climate and carbon cycle is robust, however, the magnitude of the feedback is dependent on the structure of the soil carbon model. The multi-pool carbon dynamics of RothC cause it to exhibit a slower magnitude of transient response to both increased organic carbon inputs and changes in climate compared with the one-pool model.

Gedney et al. (2004) developed an interactive wetlands scheme model that was calibrated using present-day atmospheric CH<sub>4</sub> variability. They predicted increases in global CH<sub>4</sub> flux between present day and 2100 of 75% with an increase in emissions from northern wetlands (> 30° N) of 100%, despite an estimated 10% reduction in wetland extent. This wetland response corresponds to an amplification of the total anthropogenic radiative forcing at 2100 by 3.55%.

Sitch et al. (2007) showed how elevated future tropospheric O<sub>3</sub> concentrations would have detrimental effects on plant productivity, and reduce the efficiency of the terrestrial biosphere to sequester carbon, constituting a large indirect radiative forcing of tropospheric O<sub>3</sub> on climate. Mercado et al. (2009) showed how changes in surface irradiance over the global dimming and subsequent brightening period, 1960–2000, associated with changes in anthropogenic scattering aerosols and cloud cover, led to enhanced global plant productivity and carbon storage. Scattering aerosols change both the quantity and quality (diffuse component) of surface irradiance. Diffuse light is able to penetrate further into the canopy than direct light, stimulating production in light-limited understory leaves. Mercado et al. (2009) found this diffuse radiation fertilisation effect was larger than the negative effect of reduced irradiance on global plant production. However Mercado et al. (2009) also showed local site optima in the

relationship between photosynthesis and diffuse light conditions; under heavily polluted or dark cloudy skies, plant productivity will decline as the diffuse effect is insufficient to offset decreased surface irradiance.

A comprehensive understanding and description of key ecological processes and nutrient cycles is needed in Earth system models. These include the cycles of carbon, nitrogen and phosphorus; the ecophysiological response of vegetation to changes in atmospheric composition (e.g. plant response to elevated CO<sub>2</sub> and O<sub>3</sub>, N deposition, aerosol radiation effects); the response of vegetation and soils to drought and elevated temperatures; wetland processes and methane exchange; permafrost; and wildfire disturbance. Currently, no single land surface model adequately describes all these processes.

This paper describes modelling of carbon fluxes and stores, in the vegetation and soil, as represented in version 2.2 of the Joint UK Land Environment Simulator (JULES). JULES was based on MOSES and consolidates the improved representations of key processes gained from the studies summarised in the preceding paragraphs. A companion paper (Best et al., 2011, hereafter referred to as Part 1) describes how JULES models fluxes of heat and moisture. Although they are presented separately, the fluxes of moisture and carbon are intimately linked, in particular through the stomatal resistance of the vegetation. The performance of JULES is assessed in Blyth et al. (2010).

Section 2 provides a brief overview of JULES before Sect. 3 describes the photosynthesis model, which has been substantially augmented since Cox et al. (1999) with the addition of an explicit description of light interception at different canopy-levels which leads to a multi-layer approach to scaling photosynthesis from leaf to canopy scale. The parameterisations of plant respiration and the effect of ozone on leaf photosynthesis are also covered in that section. The phenology model described in Sect. 4 is essentially unchanged since Cox et al. (1999). Section 5 outlines the simulation of soil carbon, which has changed with the introduction of a 4-pool model and the possibility of choosing between alternative descriptions of the response of heterotrophic respiration

## JULES: carbon fluxes and vegetation

D. B. Clark et al.

[Title Page](#)

[Abstract](#)

[Introduction](#)

[Conclusions](#)

[References](#)

[Tables](#)

[Figures](#)



[Back](#)

[Close](#)

[Full Screen / Esc](#)

[Printer-friendly Version](#)

[Interactive Discussion](#)



to soil temperature. A parameterisation of methane emissions from wetlands is also outlined. Finally Sect. 6 gives details of the dynamic vegetation model, TRIFFID (Cox, 2001).

## 2 Model description

JULES describes the vegetation in a gridbox using a small number of Plant Functional Types (PFTs). The default is to use 5 PFTs: broadleaf trees, needleleaf trees, C<sub>3</sub> (temperate) grasses, C<sub>4</sub> (tropical) grasses and shrubs. The surface fluxes of CO<sub>2</sub> associated with photosynthesis and plant respiration are calculated in the physiology component of JULES, as described in Sect. 3 on each JULES timestep (typically 30 to 60 min). The accumulated carbon fluxes are passed to the vegetation dynamics model (TRIFFID, described in Sect. 6) and the area covered by each PFT is updated on a longer timestep (typically 10 days) based on the net carbon available to it and on the competition with other vegetation types, which is modelled using a Lotka-Volterra approach (Cox, 2001). Leaf phenology (bud-burst and leaf drop) is updated on an intermediate timescale of 1 day, using accumulated temperature-dependent leaf turnover rates (Sect. 4). Litterfall from vegetation is input to a model of soil carbon (Sect. 5) which calculates the rate of microbial soil respiration and the consequent flux of CO<sub>2</sub> back to the atmosphere. This part of the model has changed since Cox et al. (1999) with the introduction of a 4-pool model and the possibility of choosing between alternative descriptions of the response of heterotrophic respiration to soil temperature. Methane emissions from wetlands are also calculated. After each call to TRIFFID the land surface parameters required by JULES (e.g. albedo, roughness length) are updated based on the new vegetation state, so that changes in the biophysical properties of the land surface, as well as changes in terrestrial carbon, may feed back onto the atmosphere. The land surface parameters are calculated as a function of the type, height and leaf area index of the vegetation, as described in Sect. 6.2.

## JULES: carbon fluxes and vegetation

D. B. Clark et al.

[Title Page](#)

[Abstract](#)

[Introduction](#)

[Conclusions](#)

[References](#)

[Tables](#)

[Figures](#)

[⏪](#)

[⏩](#)

[◀](#)

[▶](#)

[Back](#)

[Close](#)

[Full Screen / Esc](#)

[Printer-friendly Version](#)

[Interactive Discussion](#)



### 3 Photosynthesis

The photosynthesis model used in JULES is based upon the observed processes at the leaf scale, which are then scaled up to represent the canopy. There are three options available in JULES for scaling up to the canopy scale. These vary from the simple big leaf approach to a multi-layer canopy.

#### 3.1 Leaf biochemistry

JULES uses the biochemistry of  $C_3$  and  $C_4$  photosynthesis from Collatz et al. (1991) and Collatz et al. (1992) as applied by Sellers et al. (1996) and described in Cox et al. (1999) to determine potential (non water stressed) leaf-level photosynthesis. Leaf level photosynthesis ( $A_l$ ) is simulated as the minimum of the following three limiting rates:

1. Rubisco limited rate ( $W_c$ )

$$W_c = \begin{cases} V_{cmax} \left( \frac{c_i - \Gamma}{c_i + K_c(1 + O_a/K_o)} \right) & \text{for } C_3 \text{ plants} \\ V_{cmax} & \text{for } C_4 \text{ plants} \end{cases} \quad (1)$$

where  $V_{cmax}$  ( $\text{mol CO}_2 \text{ m}^{-2} \text{ s}^{-1}$ ) is the maximum rate of carboxylation of Rubisco,  $c_i$  (Pa) is the leaf internal carbon dioxide concentration,  $\Gamma$  (Pa) is the  $\text{CO}_2$  compensation point in the absence of mitochondrial respiration,  $O_a$  (Pa) is the partial pressure of atmospheric oxygen, and  $K_c$  and  $K_o$  (Pa) are the Michaelis-Menten constants for  $\text{CO}_2$  and  $\text{O}_2$ , respectively.

2. Light limited rate ( $W_l$ )

$$W_l = \begin{cases} \alpha(1 - \omega)I_{par} \left( \frac{c_i - \Gamma}{c_i + 2\Gamma} \right) & \text{for } C_3 \text{ plants} \\ \alpha(1 - \omega)I_{par} & \text{for } C_4 \text{ plants} \end{cases} \quad (2)$$

Title Page

Abstract

Introduction

Conclusions

References

Tables

Figures

◀

▶

◀

▶

Back

Close

Full Screen / Esc

Printer-friendly Version

Interactive Discussion



[Title Page](#)[Abstract](#)[Introduction](#)[Conclusions](#)[References](#)[Tables](#)[Figures](#)[◀](#)[▶](#)[◀](#)[▶](#)[Back](#)[Close](#)[Full Screen / Esc](#)[Printer-friendly Version](#)[Interactive Discussion](#)

where  $\alpha$  is quantum efficiency of photosynthesis ( $\text{mol CO}_2 \text{ mol}^{-1} \text{ PAR}$ ),  $I_{\text{par}}$  is the incident photosynthetically active radiation (PAR,  $\text{mol m}^{-2} \text{ s}^{-1}$ ) and  $\omega$  is the leaf scattering coefficient for PAR. The default values of PFT-specific parameters for leaf biochemistry and photosynthesis are given in Table 1.

3. Rate of transport of photosynthetic products (in the case of  $\text{C}_3$  plants) and PEP-Carboxylase limitation (in the case of  $\text{C}_4$  plants) ( $W_e$ )

$$W_e = \begin{cases} 0.5V_{\text{cmax}} & \text{for } \text{C}_3 \text{ plants} \\ 2 \times 10^4 V_{\text{cmax}} \frac{c_i}{P_*} & \text{for } \text{C}_4 \text{ plants} \end{cases} \quad (3)$$

where  $P_*$  is the surface air pressure. Parameters  $V_{\text{cmax}}$ ,  $K_o$ ,  $K_c$ , and  $\Gamma$  are all temperature dependent. JULES uses the temperature dependencies from Collatz et al. (1991, 1992).  $V_{\text{cmax}}$  at any desired temperature is calculated from the maximum rate of carboxylation of the enzyme Rubisco at  $25^\circ\text{C}$  ( $V_{\text{cmax}25}$ ) assuming an optimal temperature range as defined by PFT-specific values of parameters,  $T_{\text{upp}}$  and  $T_{\text{low}}$  as

$$V_{\text{cmax}} = \frac{V_{\text{cmax}25} f_T(T_c)}{[1 + \exp\{0.3(T_c - T_{\text{upp}})\}] [1 + \exp\{0.3(T_{\text{low}} - T_c)\}]} \quad (4)$$

where

$$f_T(T_c) = Q_{10_{\text{leaf}}}^{0.1(T_c - 25)} \quad (5)$$

$T_c$  is leaf temperature ( $^\circ\text{C}$ ) and the default value of  $Q_{10_{\text{leaf}}}$  is 2.

$V_{\text{cmax}25}$  is assumed to be linearly related to leaf nitrogen concentration,  $n_l$ :

$$V_{\text{cmax}25} = \begin{cases} 0.0008 n_l & \text{for } \text{C}_3 \text{ plants} \\ 0.0004 n_l & \text{for } \text{C}_4 \text{ plants} \end{cases} \quad (6)$$

The net (unstressed by water availability) leaf photosynthetic carbon uptake,  $A_p$ , is calculated by subtracting the leaf dark respiration ( $R_d$ ) from the gross photosynthetic rate,  $W$ :

$$W = \min(W_c, W_l, W_e) \quad (7)$$

$$R_d = f_d V_{cmax} \quad (8)$$

$$A_p = W - R_d \quad (9)$$

where  $f_d$  is the dark respiration coefficient.

Leaf photosynthesis is linked to stomatal conductance via the internal  $CO_2$  concentration, which is calculated using the Jacobs (1994) formulation. The Jacobs formulation shares similarities with the stomatal conductance formulations of Ball et al. (1987) and Leuning (1995). A description of the coupled stomatal conductance-photosynthesis model is given in Part 1 and originally in Cox et al. (1998, 1999).

To account for soil moisture stress, the potential (non-stressed) leaf photosynthesis  $A_p$  is multiplied by a soil water factor (Cox et al., 1998):

$$A_l = A_p \beta \quad (10)$$

where  $A_l$  is leaf-level photosynthesis.  $\beta$  is the moisture stress factor (unit-less) which is related to the mean soil moisture concentration in the root zone,  $\theta$ , and the critical and wilting point concentrations,  $\theta_c$  and  $\theta_w$  respectively, as follows:

$$\beta = \begin{cases} 1 & \text{for } \theta > \theta_c \\ \frac{\theta - \theta_w}{\theta_c - \theta_w} & \text{for } \theta_w < \theta \leq \theta_c \\ 0 & \text{for } \theta \leq \theta_w \end{cases} \quad (11)$$

Title Page

Abstract

Introduction

Conclusions

References

Tables

Figures

⏪

⏩

◀

▶

Back

Close

Full Screen / Esc

Printer-friendly Version

Interactive Discussion



## 3.2 Scaling photosynthesis from leaf to canopy

The description of within-canopy radiation interception and scaling from leaf to canopy-level photosynthesis has been developed considerably since Cox et al. (1999). JULES2.2 includes a process-based scaling-up of leaf-level photosynthesis to the canopy level, with alternative methods to calculate canopy radiation interception and canopy-level photosynthesis. There are two options available in JULES for scaling up from the leaf-level to the canopy scale: (i) the canopy is considered as a big leaf and (ii) a multi-layer canopy. Within the multi-layer option, JULES has four variations that depend on considerations of vertical gradients of canopy photosynthetic capacity, inclusion of light inhibition of leaf respiration, inclusion of sunfleck penetration and splitting canopy layers into sunlit and shaded leaves. All options are described below and summarised in Table 2.

### 3.2.1 Big leaf approach

#### Radiation interception and scaling up to canopy-level

In the big leaf approach, incident radiation attenuates through the canopy following Beer's law (Monsi and Saeki, 1953)

$$I_c = I_0 e^{-kL_c} \quad (12)$$

where  $I_c$  is irradiance beneath the canopy,  $I_0$  irradiance at the top of the canopy,  $L_c$  is the canopy leaf area index and  $k$  is a light extinction coefficient.

Leaf-level photosynthetic capacity is assumed to vary proportionally with the vertical distribution of irradiance (Sellers et al., 1992), therefore leaf photosynthesis  $A_l$  can also be expressed as a function of the top of the canopy leaf photosynthesis  $A_0$ , leaf area index  $L$  and the light extinction coefficient:

$$A_l = A_0 e^{-kL} \quad (13)$$

**GMDD**

4, 641–688, 2011

## JULES: carbon fluxes and vegetation

D. B. Clark et al.

Title Page

Abstract

Introduction

Conclusions

References

Tables

Figures

◀

▶

◀

▶

Back

Close

Full Screen / Esc

Printer-friendly Version

Interactive Discussion



Canopy photosynthesis is calculated as the integral of leaf-level photosynthesis over the entire canopy leaf area index:

$$A_c = \int_0^{L_c} A_l dL = A_o \left[ 1 - e^{-kL_c} \right] / k \quad (14)$$

Canopy-level conductance and respiration are estimated using similar expressions.

### 5 3.2.2 Multi-layer approach

#### Radiation interception

The canopy is divided into a number of layers ( $n$ , typically 10) of equal leaf area increments  $dL_c = L_c/n$ . JULES adopts the two-stream approximation of radiation interception from Sellers (1985) to calculate surface spectral albedos (Essery et al., 2001) and the absorbed incoming radiation for each canopy layer. The absorbed incident PAR at each layer varies with solar zenith angle, incident direct and diffuse radiation at the top of the canopy, canopy leaf angle distribution and leaf radiation properties in the visible and near-infrared wavebands. JULES explicitly describes absorption and scattering of both direct and diffuse radiation fluxes separately in the visible and near-infrared wavebands at each canopy layer, which leads to the calculation of upward and downward diffuse fluxes of scattered direct beam radiation ( $I_{dir} \uparrow_i, I_{dir} \downarrow_i$ ) and incident diffuse radiation and scattered diffuse radiation ( $I_{dif} \uparrow_i, I_{dif} \downarrow_i$ ) per canopy layer. These fluxes are then used to calculate the direct and diffuse fractions of absorbed incident PAR,  $FAPAR_{DIR_i}$  and  $FAPAR_{DIF_i}$ , at each canopy layer  $i$ :

$$FAPAR_{DIR_i} = [I_{dir} \uparrow_i - I_{dir} \downarrow_i] dL_c \quad (15)$$

$$FAPAR_{DIF_i} = [I_{dif} \uparrow_i - I_{dif} \downarrow_i] dL_c \quad (16)$$

A comparison of the vertical profile of absorbed incident PAR calculated with the two-stream approach against the profile estimated with Beer's law showed that the results

Title Page

Abstract

Introduction

Conclusions

References

Tables

Figures

◀

▶

◀

▶

Back

Close

Full Screen / Esc

Printer-friendly Version

Interactive Discussion



were similar only when the incident PAR was a direct beam coming from a high sun angle, otherwise the fraction of absorbed PAR at any canopy-level is higher when calculated using Beer's law (Jogireddy et al., 2006).

The two-stream approach provides a vertical profile of intercepted radiation within the canopy which allows estimation of photosynthesis and leaf respiration for each leaf area increment within the canopy.

### Sunfleck penetration

A further improvement to the estimation of absorbed radiation fluxes within the canopy considers penetration of sunflecks through the canopy, which corresponds to the direct component of the direct beam radiation  $I_b$ , i.e. it excludes the scattering component. Such a term is not included in Eq. (15). Thus, attenuation of non-scattered incident beam radiation per unit leaf area at canopy depth  $L$  is (Dai et al., 2004):

$$I_b = I_{b_0} (1 - \omega) k_b \exp^{-k_b L} \quad (17)$$

where  $I_{b_0}$  is incident direct radiation,  $(1 - \omega)$ , is the non-scattered part of the incident beam (i.e. what is absorbed) and  $k_b$  is the canopy beam radiation extinction coefficient.

Following Dai et al. (2004) as implemented in Mercado et al. (2009), radiation fluxes are split into direct beam radiation, scattered direct beam and diffuse radiation and it is assumed that sunlit leaves absorb all types of radiation, while shaded leaves absorb only diffuse radiation. The fraction of sunlit leaves ( $f_{\text{sun}}$ ), is defined as:

$$f_{\text{sun}} = \exp^{-k_b L} \quad (18)$$

For each canopy layer  $i$  with leaf area increment within the canopy ( $dL_c$ ), the fraction of sunlit leaves, absorbed direct beam radiation ( $I_{b_i}$ ), scattered direct beam ( $I_{bs_i}$ ) and diffuse radiation ( $I_{d_i}$ ) is calculated as:

$$f_{\text{sun}_i} = \frac{\exp^{-k_b L} (\exp^{-k_b d_c} - 1)}{k_b d L_c} \quad (19)$$

Title Page

Abstract

Introduction

Conclusions

References

Tables

Figures

◀

▶

◀

▶

Back

Close

Full Screen / Esc

Printer-friendly Version

Interactive Discussion



$$I_{b_i} = (1 - \omega) \left( \frac{\exp^{-k_b(L-dL_c)} - \exp^{-k_bL}}{dL_c} \right) \quad (20)$$

$$I_{bs_i} = \omega \left( \frac{\exp^{-k_b(L-dL_c)} - \exp^{-k_bL}}{dL_c} \right) + \text{FAPAR}_{\text{DIR}_i} \quad (21)$$

$$I_{d_i} = \text{FAPAR}_{\text{DIF}_i} \quad (22)$$

The fraction of radiation absorbed by sunlit leaves  $I_{\text{sun}_i}$  and shaded leaves  $I_{\text{sh}_i}$  at each leaf area increment within the canopy is calculated as:

$$I_{\text{sh}_i} = f_d I_{d_i} + (1 - f_d) I_{bs_i} \quad (23)$$

$$I_{\text{sun}_i} = I_{\text{sh}_i} + (1 - f_d) I_{b_i} / f_{\text{sun}_i} \quad (24)$$

where  $f_d$  is the fraction of PAR which is diffuse radiation.  $I_{\text{sun}_i}$  and  $I_{\text{sh}_i}$  are used to estimate photosynthesis from sunlit  $A_{\text{sun}_i}$  and shaded leaves  $A_{\text{sh}_i}$  for each leaf area increment within the canopy.

### Scaling up to canopy-level

Canopy-scale fluxes are estimated as the sum of the leaf-level fluxes in each layer scaled by leaf area. Hence canopy-level photosynthesis is estimated from layer leaf-level photosynthesis ( $A_{ij}$ ) as follows:

$$A_j = A_{ij} dL_c \quad (25)$$

$$A_c = \sum_{i=0}^n A_j \quad (26)$$

with  $A_j$  as photosynthesis from each canopy layer. When including sunflecks and accounting explicitly for photosynthesis by sunlit and shaded leaves,  $A_j$  is calculated as

$$A_j = f_{\text{sun}_j} A_{\text{sun}_j} + (1 - f_{\text{sun}_j}) A_{\text{sh}_j} \quad (27)$$

Canopy respiration and conductance are estimated in a similar manner.

## GMDD

4, 641–688, 2011

### JULES: carbon fluxes and vegetation

D. B. Clark et al.

Title Page

Abstract

Introduction

Conclusions

References

Tables

Figures

◀

▶

◀

▶

Back

Close

Full Screen / Esc

Printer-friendly Version

Interactive Discussion



## Photosynthetic capacity at each canopy layer

The multi-layer scheme has been applied and tested against eddy correlation flux measurements (Mercado et al., 2007) using different assumptions of the vertical distribution of leaf nitrogen. Such a distribution is a proxy for the vertical distributions of photosynthetic capacity  $V_{\text{cmax}}$  and leaf respiration through the canopy. The distributions tested were a uniform distribution with leaf N constant through the canopy, and a distribution with leaf N decreasing from top to bottom of the canopy. In the latter case, the vertical profiles of leaf N, photosynthetic capacity and leaf respiration within the canopy were estimated following de Pury and Farquhar (1997) using measured vertical profiles from a rainforest site in the Amazon Basin (Carswell et al., 2000) and prescribed in JULES to decrease exponentially with increasing canopy depth (Mercado et al., 2007).

Photosynthetic capacity ( $V_{\text{cmax},i}$ ) at each canopy layer  $i$  is estimated as

$$V_{\text{cmax},i} = N_0 n_e \exp^{-k_n i/n} \quad (28)$$

with  $N_0$  the leaf  $N$  concentration at the top of the canopy and  $k_n$  a nitrogen allocation coefficient estimated to be 0.78.  $n_e$  is a constant that linearly relates leaf  $N$  concentration to Rubisco carboxylation capacity, with values of 0.0008 and 0.0004 for  $C_3$  and  $C_4$  plants, respectively. These values were derived from Shulze et al. (1994) assuming that 40 percent of the total leaf carbon mass is dry matter and that maximum rate of photosynthetic uptake is half of maximum photosynthetic capacity (Cox, 2001). Vertical profiles of  $V_{\text{cmax}}$  remain to be tested further and evaluated for other vegetation types.

An additional process is included in the multi-layer version of JULES which accounts for inhibition of leaf respiration in the light. Mercado et al. (2007) tested the inclusion of inhibition of leaf respiration by the light from Brooks and Farquhar (1985) as implemented by Lloyd et al. (1995) for a rainforest site in the Amazon. Once JULES was correctly parameterised for canopy photosynthetic capacity at this site, the inclusion of this inhibition allowed much better predictions of observed rates of net photosynthetic uptake.

**GMDD**

4, 641–688, 2011

## JULES: carbon fluxes and vegetation

D. B. Clark et al.

Title Page

Abstract

Introduction

Conclusions

References

Tables

Figures

◀

▶

◀

▶

Back

Close

Full Screen / Esc

Printer-friendly Version

Interactive Discussion



### 3.2.3 Assessment of big-leaf and multi-layer approaches

JULES was evaluated using the multi-layer approach and eddy correlation data for a temperate coniferous forest site in the Netherlands (Jogireddy et al., 2006) and a tropical broad leaf rainforest site in the Brazilian Amazon (Mercado et al., 2007). Both studies demonstrated the superior performance of the multi-layer approach with the two-stream canopy radiation interception (Sellers, 1985) compared to the big-leaf approach in simulating canopy scale photosynthetic fluxes, specifically both the simulated light response and diurnal cycles of photosynthesis. Further evaluation of the multi-layer approach at eddy correlation sites and globally is presented in Blyth et al. (2010).

The multi-layer approach has been applied using different assumptions for the number of canopy layers (either 2 or 10). Jogireddy et al. (2006) compared simulated canopy photosynthesis using two and ten layers at a coniferous forest site, and found the 2-layer option to give a good fit to the 10-layer simulation. Because the two layer option is computationally efficient, Jogireddy et al. (2006) recommended this option for large scale applications if computer resources are limited. Allowing leaf nitrogen, canopy photosynthetic capacity and leaf respiration to vary through the canopy, provides a more realistic representation of canopy and total plant respiration in JULES; the description of stem and root respiration in JULES is a dependent function of canopy respiration and their respective nitrogen contents. This is especially apparent in tropical ecosystems, where simulations which assume a uniform vertical distribution of leaf N, and therefore photosynthetic capacity, produce very large respiration fluxes from leaves in the shaded understorey. Observations of a decrease of leaf N and photosynthetic capacity within canopies (Meir et al., 2002) and decrease of leaf respiration in the light (Brooks and Farquhar, 1985; Atkin et al., 1998; Hoefnagel et al., 1998; Atkin et al., 2000) support their inclusion into JULES.

Use of the two-stream canopy radiation interception scheme and multi-layer approach to photosynthesis provides realistic representation of the light response of

## GMDD

4, 641–688, 2011

### JULES: carbon fluxes and vegetation

D. B. Clark et al.

[Title Page](#)

[Abstract](#)

[Introduction](#)

[Conclusions](#)

[References](#)

[Tables](#)

[Figures](#)

[⏪](#)

[⏩](#)

[◀](#)

[▶](#)

[Back](#)

[Close](#)

[Full Screen / Esc](#)

[Printer-friendly Version](#)

[Interactive Discussion](#)



photosynthesis and its diurnal cycle, and having a non-uniform distribution of canopy photosynthetic capacity produces more realistic estimates of canopy and plant respiration. Also the scheme allows differentiation between direct and diffuse radiation, which is not possible using the Beer's law approach. Figure 1 shows evaluation of Gross Primary Productivity (GPP) simulated by JULES using eddy correlation data from a temperate broad leaf (Knobl et al., 2003) and a needle leaf (Rebmann et al., 2010) site. Observations are compared against JULES using the big leaf approach and the multi-layer option that includes vertical decrease of photosynthetic capacity and inclusion of light inhibition of leaf respiration (options 1 and 4 in Table 2). The multi-layer approach shows a more realistic light response and diurnal cycle of photosynthesis than the big leaf approach.

Inclusion of sun fleck provided a platform to study the differential effects of direct and diffuse radiation on carbon and water exchange. A global model application of the effects of diffuse radiation on the land carbon sink (Mercado et al., 2009) uses ten canopy layers and non-uniform distribution of photosynthetic capacity through the canopy. The 10-layer model, including sunfleck penetration, the vertical decrease in photosynthetic capacity within the canopy and the inhibition of respiration in the light, is the recommended default setting (option 5 Table 2) for applications at all scales from individual sites to global modelling. This is because it provides the most realistic representation of plant physiological processes. However, the inclusion of a vertical profile of photosynthetic capacity through the canopy is likely to require specific parameterisations for each PFT. In addition, the percentage inhibition of leaf respiration in the light is based on limited data for a small number of species. More observational data are needed to refine this inhibition and how it varies across plant functional types. These will be the focus of future model development.

### 3.3 Ozone effects on photosynthesis

Ozone causes cellular damage inside leaves which adversely affects plant production, reduces photosynthetic rates and requires increased resource allocation to detoxify

## JULES: carbon fluxes and vegetation

D. B. Clark et al.

[Title Page](#)

[Abstract](#)

[Introduction](#)

[Conclusions](#)

[References](#)

[Tables](#)

[Figures](#)

[◀](#)

[▶](#)

[◀](#)

[▶](#)

[Back](#)

[Close](#)

[Full Screen / Esc](#)

[Printer-friendly Version](#)

[Interactive Discussion](#)



and repair leaves (Ashmore, 2005). JULES uses a flux-gradient approach to model ozone damage, following Sitch et al. (2007). It is assumed that ozone suppresses the potential net leaf photosynthesis in proportion to the ozone flux through stomata above a specified critical ozone deposition flux, so that the actual net photosynthesis ( $A$ ) is given by

$$A = A_p F \quad (29)$$

where the reduction factor

$$F = 1 - a \max [F_{O_3} - F_{O_3 \text{ crit}}, 0] \quad (30)$$

is given by the instantaneous leaf uptake of  $O_3$  over a plant type-specific threshold,  $F_{O_3 \text{ crit}}$ , in  $\text{nmol m}^{-2} \text{s}^{-1}$ , multiplied by a plant-specific parameter ( $a$ ), following Pleijel et al. (2004). The cumulative effect of leaf damage and early senescence is implicitly accounted for in our calibration of  $a$  (by compensating a shortened growing season by reducing photosynthesis).

The flux  $F_{O_3}$  is calculated by analogy with Ohm's law as

$$F_{O_3} = \frac{[O_3]}{r_a + \kappa_{O_3} / g_l} \quad (31)$$

where  $[O_3]$  is the molar concentration of  $O_3$  at reference level ( $\text{nmol m}^{-3}$ ),  $r_a$  is the aerodynamic and boundary layer resistance between leaf surface and reference level ( $\text{s m}^{-1}$ ),  $g_l$  is the leaf conductance for  $H_2O$  ( $\text{m s}^{-1}$ ), and  $\kappa_{O_3} = 1.67$  is the ratio of leaf resistance for  $O_3$  to leaf resistance for water vapour. The uptake flux is dependent on the stomatal conductance, which is dependent on the photosynthetic rate in JULES. Given  $g_l$  is a linear function of photosynthetic rate (Eq. 13, Cox et al., 1999), from Eq. (29) it follows that

$$g_l = g_p F \quad (32)$$

## GMDD

4, 641–688, 2011

### JULES: carbon fluxes and vegetation

D. B. Clark et al.

Title Page

Abstract

Introduction

Conclusions

References

Tables

Figures

◀

▶

◀

▶

Back

Close

Full Screen / Esc

Printer-friendly Version

Interactive Discussion



where  $g_p$  is the leaf conductance in the absence of  $O_3$  effects. Through this mechanism the direct effect of  $O_3$  deposition on photosynthesis also leads to a reduction in stomatal conductance. As the  $O_3$  flux itself depends on the stomatal conductance, which in turn depends upon the net rate of photosynthesis (Cox et al., 1999), the model requires a consistent solution for the net photosynthesis, stomatal conductance and the ozone deposition flux. Equations (30–32) produce a quadratic in  $F$  which is solved analytically.

Data from field observation (Karlsson et al., 2004; Pleijel et al., 2004) are used to calibrate plant-ozone effects for the five standard PFTs described by JULES (see Sitch et al. (2007) for details of the calibration procedure and Table 3 for parameter values). Sitch et al. (2007) presented “high” and “low” parameterisations for each PFT to represent species sensitive and less sensitive, respectively, to ozone effects. The default parameter values in JULES are the “low” sensitivity values. Threshold values,  $F_{O_3 \text{ crit}}$ , are taken at 1.6 and 5  $\text{nmol m}^{-2} \text{s}^{-1}$  for the woody and grass PFTs, respectively. Although a threshold of 5 implies a smaller  $O_3$  dose for grasses, the gradient of the dose-response function ( $a$ ), is larger, and therefore grasses may become more sensitive to ozone exposure than trees at high ozone concentrations. For shrubs we assume the same plant-ozone sensitivity as broad-leaf trees.

### 3.4 Plant respiration

Plant respiration,  $R_p$ , is split into maintenance and growth respiration (Cox et al., 1999):

$$R_p = R_{pm} + R_{pg} \quad (33)$$

Growth respiration is assumed to be a fixed fraction of the net primary productivity, thus:

$$R_{pg} = r_g (\Pi_G - R_{pm}) \quad (34)$$

where  $\Pi_G$  is the gross primary productivity, and the growth respiration coefficient is set to  $r_g = 0.25$  for all PFTs. Leaf maintenance respiration is equivalent to the moisture modified canopy dark respiration,  $\beta R_{dc}$ , while root and stem respiration is assumed

Title Page

Abstract

Introduction

Conclusions

References

Tables

Figures

◀

▶

◀

▶

Back

Close

Full Screen / Esc

Printer-friendly Version

Interactive Discussion



to be independent of soil moisture, but to have the same dependences on nitrogen content and temperature. Thus total maintenance respiration is given by:

$$R_{pm} = 0.012R_{dc} \left( \beta + \frac{(N_r + N_s)}{N_l} \right) \quad (35)$$

where  $N_l$ ,  $N_s$  and  $N_r$  are the nitrogen contents of leaf, stem and root, and the factor of 0.012 converts from ( $\text{mol CO}_2 \text{ m}^{-2} \text{ s}^{-1}$ ) to ( $\text{kg C m}^{-2} \text{ s}^{-1}$ ). The nitrogen contents are given by:

$$N_l = n_l \sigma_l L \quad (36)$$

$$N_r = \mu_{rl} n_l \mathcal{R} \quad (37)$$

$$N_s = \mu_{sl} n_l \mathcal{S} \quad (38)$$

where  $n_l$  is the mean leaf nitrogen concentration ( $\text{kg N (kg C)}^{-1}$ ),  $\mathcal{R}$  and  $\mathcal{S}$  are the carbon contents of respiring root and stem,  $L$  is the canopy leaf area index and  $\sigma_l$  ( $\text{kg C m}^{-2}$ ) is the specific leaf density. The nitrogen concentrations of roots and stem are assumed to be fixed (functional type dependent) multiples,  $\mu_{rl}$  and  $\mu_{sl}$ , of the mean leaf nitrogen concentration:  $\mu_{rl} = 1.0$  for all PFTS,  $\mu_{sl} = 0.1$  for woody plants (trees and shrubs) and  $\mu_{sl} = 1.0$  for grasses. The respiring stemwood is calculated using a “pipemodel” approach in which live stemwood is proportional to leaf area  $L$  and canopy height,  $h$ :

$$\mathcal{S} = 0.01 h L \quad (39)$$

The constant of proportionality is approximated from Friend et al. (1993).

## 4 Leaf phenology

Leaf phenology is modelled as described in Cox (2001). Leaf mortality rates,  $\gamma_{lm}$ , for the tree-PFTs are assumed to be a function of temperature, increasing from a minimum

Title Page

Abstract

Introduction

Conclusions

References

Tables

Figures

◀

▶

◀

▶

Back

Close

Full Screen / Esc

Printer-friendly Version

Interactive Discussion



value of  $\gamma_0$ , as the leaf temperature drops below a threshold value,  $T_{\text{off}}$ :

$$\gamma_{\text{lm}} = \begin{cases} \gamma_0 & \text{for } T > T_{\text{off}} \\ \gamma_0 \{1 + d_T(T_{\text{off}} - T)\} & \text{for } T \leq T_{\text{off}} \end{cases} \quad (40)$$

$d_T$  is the rate of change of  $\gamma_{\text{lm}}$  with respect to temperature, and equals 9 by default (Table 4) meaning that the leaf turnover rate increases by a factor of 10 when the temperature drops 1 °C below  $T_{\text{off}}$ . Equation (40) describes how leaf mortality varies with temperature, but it is not sufficient to produce realistic phenology. A variable,  $\rho$ , is introduced which describes the phenological status of the vegetation:

$$L = \rho L_b \quad (41)$$

where  $L$  is the actual LAI of the canopy, and  $L_b$  is the balanced (or seasonal maximum) LAI as updated by the dynamic vegetation model (TRIFFID) via the inverse of Eq. (64). The phenological status,  $\rho$ , is updated typically on a daily basis assuming:

- leaves are dropped at a constant absolute rate ( $\gamma_\rho L_b$ ) when the mean value of leaf turnover, as given by Eq. (40), exceeds twice its minimum value
- budburst occurs at the same rate when  $\gamma_{\text{lm}}$  drops back below this threshold, and “full leaf” is approached asymptotically thereafter:

$$\frac{d\rho}{dt} = \begin{cases} -\gamma_\rho & \text{for } \gamma_{\text{lm}} > 2\gamma_0 \\ \gamma_\rho(1 - \rho) & \text{for } \gamma_{\text{lm}} \leq 2\gamma_0 \end{cases} \quad (42)$$

where  $\gamma_\rho = 20 \text{ yr}^{-1}$ . The effective leaf turnover rate,  $\gamma_1$ , as used in Eq. (65), must also be updated to ensure conservation of carbon when phenological changes are occurring:

$$\gamma_1 = \begin{cases} -\frac{d\rho}{dt} & \text{for } \gamma_{\text{lm}} > 2\gamma_0 \\ \rho\gamma_{\text{lm}} & \text{for } \gamma_{\text{lm}} \leq 2\gamma_0 \end{cases} \quad (43)$$

Taken together, Eqs. (40), (42) and (43) amount to a “chilling-days” parameterisation of leaf phenology. Cold-deciduous behaviour can effectively be disabled for any of the

Title Page

Abstract

Introduction

Conclusions

References

Tables

Figures

◀

▶

◀

▶

Back

Close

Full Screen / Esc

Printer-friendly Version

Interactive Discussion



PFTs by setting parameter  $d_T$  to zero for that PFT. A similar approach exists in the JULES code for drought-deciduous phenology involving equations similar to Eq. (40) but for leaf turnover as a function of soil moisture, with a parameter  $d_M$ . However, this is considered to be still under development and default parameters of  $d_M = 0$  for all PFTs mean that this is effectively switched off for general use.

Calculation of leaf phenology is independent of the calculation of the evolution of vegetation coverage and can be included even when the dynamic vegetation component, TRIFFID, is turned off.

## 5 Soil carbon

Total soil carbon storage,  $C_s$ , is increased by the total litterfall,  $\Lambda_c$ , and reduced by microbial soil respiration,  $R_s$ , which returns  $\text{CO}_2$  to the atmosphere:

$$\frac{dC_s}{dt} = \Lambda_c - R_s \quad (44)$$

In each gridbox, the total litterfall is made-up of the area-weighted sum of the local litterfall from each PFT (as given by Eq. 65), along with terms due to the large-scale disturbance rate,  $\gamma_v$ , and PFT competition (from the TRIFFID dynamic vegetation model, see Sect. 6):

$$\Lambda_c = \sum_i v_i \left( \Lambda_{li} + \gamma_{vi} C_{vi} + \Pi_i \sum_j c_{ij} v_j \right) \quad (45)$$

The competition term (last term on the right-hand side of Eq. 45) is derived by imposing carbon conservation on the soil-vegetation system as described by Eq. (57), (58) and (44). It implies that the NPP of each PFT will be lost entirely as litter once the PFT occupies all of the space available to it (i.e. when  $\sum_j c_{ij} v_j = 1$ ).

If the TRIFFID DGVM is used, four soil pools are modelled, otherwise a single pool with a fixed (in time) value is used (Cox, 2001) to calculate soil respiration. However,

Title Page

Abstract

Introduction

Conclusions

References

Tables

Figures

◀

▶

◀

▶

Back

Close

Full Screen / Esc

Printer-friendly Version

Interactive Discussion



in this case the soil carbon pool is not updated and net carbon fluxes may not be in balance. It is recommended that TRIFFID is used if simulation of soil carbon fluxes is required.

## 5.1 Implementation of the RothC soil carbon model

5 The soil carbon model comprises 4 carbon pools and follows the formulation of the RothC soil carbon scheme (Jenkinson, 1990; Coleman and Jenkinson, 1999). Plant input is split between two carbon pools of decomposable (DPM) and resistant (RPM) plant material depending on the overlying vegetation type, with grasses providing a higher fraction of decomposable litter input and trees a higher fraction of resistant  
10 litter input. The other two carbon pools represented are a microbial biomass (BIO) and a long-lived humified pool (HUM).

Respiration from each soil carbon pool is the product of a specific respiration rate,  $\kappa_{si}$ , (the rate of respiration of unit mass of that pool under standard conditions), the pool size,  $C_i$ , and several rate modifying factors.

$$15 R_i = \kappa_{si} C_i F_T(T_{soil}) F_\theta(\theta) F_v(v) \quad (46)$$

Values of  $\kappa_{si}$  for each pool are given in Table 5. The rate modifying factors,  $F$ , account for the effects of soil temperature,  $T_{soil}$ , soil moisture,  $\theta$ , and vegetation fractional cover ( $v$ ) on heterotrophic respiration. The form of the temperature rate modifier is controlled by a switch which selects between a  $Q_{10}$  function:

$$20 F_T(T_{soil}) = Q_{10\_soil}^{(T_{soil}-298.15)/10} \quad (47)$$

where the default value is  $Q_{10\_soil} = 2.0$ , and the RothC temperature function (Jenkinson, 1990):

$$F_T(T_{soil}) = \frac{47.9}{1 + \exp[106/(T_{soil} - 254.85)]} \quad (48)$$

Title Page

Abstract

Introduction

Conclusions

References

Tables

Figures

◀

▶

◀

▶

Back

Close

Full Screen / Esc

Printer-friendly Version

Interactive Discussion



The temperature of the top soil layer (typically 10 cm deep) is used in both cases. Figure 2 compares these alternative temperature functions.

The effect of soil moisture is described as

$$f_{\theta} = \begin{cases} 1 - 0.8(S - S_o) & \text{for } S > S_o \\ 0.2 + 0.8 \left( \frac{S - S_{\min}}{S_o - S_{\min}} \right) & \text{for } S_{\min} < S \leq S_o \\ 0.2 & \text{for } S \leq S_{\min} \end{cases} \quad (49)$$

- 5 where  $S$  and  $S_o$  are the unfrozen soil moisture content of the top soil layer and the optimum soil moisture, both expressed as a fraction of saturation.  $S_o = 0.5(1 + S_w)$  and  $S_{\min} = 1.7S_w$ , where  $S_w$  is the soil moisture at wilting point. The general form of the moisture function from Cox (2001) has been retained in preference to the RothC moisture function because of its ability to simulate reduced respiration in very wet soils.
- 10 However, it has been revised (the original set  $S_{\min} = S_w$ ) so as to simulate a greater sensitivity of respiration reduction in dry soils, which gave a better fit to the observed site-level seasonal cycle of respiration. The importance of moisture controls on future soil carbon is discussed in Jones and Falloon (2009).

The effect of vegetation cover is described as

$$15 \quad F_v(v) = 0.6 + 0.4 \cdot (1 - v) \quad (50)$$

varying linearly from 0.6 under fully vegetated soil to 1 under completely bare soil.

The carbon pools are updated according to

$$d(\text{DPM})/dt = \alpha_{\text{dr}} \Lambda_c - R_{\text{DPM}} \quad (51)$$

$$d(\text{RPM})/dt = (1 - \alpha_{\text{dr}}) \Lambda_c - R_{\text{RPM}} \quad (52)$$

$$20 \quad d(\text{BIO})/dt = 0.46 \cdot \beta R_s - R_{\text{BIO}} \quad (53)$$

$$d(\text{HUM})/dt = 0.54 \cdot \beta R_s - R_{\text{HUM}} \quad (54)$$

where  $R_s$  is the total respiration rate, summed over the 4 pools, the final  $R_i$  terms are respiration rates for each pool, and  $\alpha_{\text{dr}}$  controls the ratio of litter input to DPM

Title Page

Abstract

Introduction

Conclusions

References

Tables

Figures

⏪

⏩

◀

▶

Back

Close

Full Screen / Esc

Printer-friendly Version

Interactive Discussion



and RPM, taking values of 0.25 for trees, 0.33 for shrubs, 0.67 for natural grass and 1.44 for crops.  $\beta$  depends on soil texture to account for the protective effect of small particle sizes. Carbon from decomposition of all 4 carbon pools is partly released to the atmosphere and partly feeds the BIO and HUM pools.

5 It is expected that the inclusion of multi-pool dynamics in the soil carbon model will dampen the transient response of soil carbon storage to both changes in litter input and changes in climate (Jones et al., 2005), although the long-term sensitivity will be unchanged if the same  $Q_{10}$  function of sensitivity to temperature is used.

## 5.2 Methane emissions from wetlands

10 The methane emission from the wetland fraction of each gridbox is calculated following Gedney et al. (2004) as:

$$F_{\text{CH}_4} = f_{\text{wet}} k_{\text{CH}_4} C_{\text{eff}} Q_{10\text{-CH}_4}^{0.1(T_{\text{soil}} - T_0)} \quad (55)$$

15 where  $k_{\text{CH}_4}$  is a global constant,  $C_{\text{eff}}$  is the effective substrate availability,  $Q_{10\text{-CH}_4}$  is a temperature-dependent  $Q_{10}$  factor and  $T_0$  is a reference temperature.  $f_{\text{wet}}$  is the fraction of the gridbox that is considered to be wetland (i.e. stagnant water) and is calculated using subgrid topographic information, as described in Part 1. The effective  $Q_{10}$  value is calculated as

$$Q_{10\text{-CH}_4}(T) = Q_{10\text{-CH}_4}(T_0)^{T_0/T} \quad (56)$$

20 When the four-pool soil carbon model is used the substrate availability is calculated by weighting the size of each pool by its specific respiration rate, otherwise  $C_{\text{eff}} = C_s$ . The default parameter values are  $k_{\text{CH}_4} = 7.4 \times 10^{-12} \text{ kg m}^{-2} \text{ s}^{-1}$ ,  $T_0 = 273.15 \text{ K}$  and  $Q_{10\text{-CH}_4}(T_0) = 3.7$ .

Title Page

Abstract

Introduction

Conclusions

References

Tables

Figures

⏪

⏩

◀

▶

Back

Close

Full Screen / Esc

Printer-friendly Version

Interactive Discussion



## 6 Vegetation dynamics

The dynamic vegetation model used in JULES is TRIFFID (Cox, 2001). Each land grid box is assumed to be either completely ice-covered (in which case TRIFFID is not used) or to have no ice cover. At these non-ice points, the urban and lake surface types (if present) are assumed to have time-constant fractions while the 5 PFTs compete for coverage as simulated by TRIFFID. The final surface type, bare soil, is the remaining space after simulating the coverage of the vegetation types.<sup>1</sup>

### 6.1 Vegetation growth and competition

The vegetation carbon density,  $C_v$ , and fractional coverage,  $v$ , of a given PFT are updated based on the carbon balance of that PFT and on competition with other PFTs:

$$\frac{dC_v}{dt} = (1 - \lambda)\Pi - \Lambda_l \quad (57)$$

$$C_v \frac{dv}{dt} = \lambda \Pi v_* \left( 1 - \sum_j c_{ij} v_j \right) - \gamma_v v_* C_v \quad (58)$$

where  $v_* = \max\{v, 0.01\}$ ,  $\Pi$  is the net primary productivity per unit vegetated area of the PFT in question and  $\gamma_v$  is the large-scale disturbance rate. Default values of PFT-specific parameters for TRIFFID are given in Table 6. A fraction  $\lambda$  of this NPP is utilised in increasing the fractional coverage (Eq. 58), and the remainder increases the carbon content of the existing vegetated area (Eq. 57). Under most circumstances the variable  $v_*$  is identical to the areal fraction,  $v$ , but each PFT is “seeded” by ensuring that  $v_*$  never drops below the “seed fraction” of 0.01.

<sup>1</sup>Note that although the number of PFTs in JULES is generally flexible, TRIFFID can only use the 5 standard PFTs (broadleaf trees, needleleaf trees,  $C_3$  grasses,  $C_4$  grasses and shrubs) as the competition coefficients are hardwired.

**GMDD**

4, 641–688, 2011

## JULES: carbon fluxes and vegetation

D. B. Clark et al.

Title Page

Abstract

Introduction

Conclusions

References

Tables

Figures

◀

▶

◀

▶

Back

Close

Full Screen / Esc

Printer-friendly Version

Interactive Discussion



**JULES: carbon fluxes  
and vegetation**

D. B. Clark et al.

[Title Page](#)[Abstract](#)[Introduction](#)[Conclusions](#)[References](#)[Tables](#)[Figures](#)[◀](#)[▶](#)[◀](#)[▶](#)[Back](#)[Close](#)[Full Screen / Esc](#)[Printer-friendly Version](#)[Interactive Discussion](#)

The competition coefficients,  $c_{ij}$ , represent the impact of vegetation type  $j$  on the vegetation type of interest. These coefficients all lie between zero and unity, so that competition for space acts to reduce the growth of  $v$  that would otherwise occur (i.e. it produces density-dependent litter production). Each PFT experiences “intra-species” competition, with  $c_{ii} = 1$  so that vegetation fraction is always limited to be less than one. Competition between natural PFTs is based on a tree-shrub-grass dominance hierarchy, with dominant types  $i$  limiting the expansion of sub-dominant types  $j$  ( $c_{ji} = 1$ ), but not vice-versa ( $c_{ij} = 0$ ). However, the tree types (broadleaf and needleleaf) and grass types ( $C_3$  and  $C_4$ ) co-compete with competition coefficients dependent on their relative heights,  $h_i$  and  $h_j$ :

$$c_{ij} = \frac{1}{1 + \exp\{20(h_i - h_j)/(h_i + h_j)\}} \quad (59)$$

The form of this function ensures that the  $i$ th PFT dominates when it is much taller, and the  $j$ th PFT dominates in the opposite limit. The factor of 20 was chosen to give co-competition over a reasonable range of height differences. Some allowance is made for agricultural regions, from which the woody types (i.e. trees and shrubs) are excluded, and only  $C_3$  and  $C_4$  grasses can grow. These can be interpreted as “crops” but are not simulated differently in agricultural or non-agricultural regions.

The  $\lambda$  partitioning coefficient in Eqs. (57) and (58) is assumed to be piecewise linear in the leaf area index, with all of the NPP being used for growth for small LAI values, and all the NPP being used for “spreading” for large LAI values:

$$\lambda = \begin{cases} 1 & \text{for } L_b > L_{\max} \\ \frac{L_b - L_{\min}}{L_{\max} - L_{\min}} & \text{for } L_{\min} < L_b \leq L_{\max} \\ 0 & \text{for } L_b \leq L_{\min} \end{cases} \quad (60)$$

where  $L_{\max}$  and  $L_{\min}$  are parameters describing the maximum and minimum leaf area

index values for the given plant functional type, and  $L_b$  is the “balanced” LAI which would be reached if the plant was in “full leaf”. The actual LAI depends on  $L_b$  and the phenological status of the vegetation type, which is updated as a function of temperature (see Sect. 4).

As the DGVM component of JULES, TRIFFID simulates the evolution of both the fractional coverage of vegetation and of terrestrial carbon storage. An option exists to disable updating of the vegetation fractions so that JULES can be run with fixed surface cover but evolving carbon storage.

Changes in vegetation carbon density,  $C_v$ , are related allometrically to changes in the balanced LAI,  $L_b$ . First,  $C_v$  is broken down into leaf,  $\mathcal{L}$ , root,  $\mathcal{R}$ , and total stem carbon,  $\mathcal{W}$ :

$$C_v = \mathcal{L} + \mathcal{R} + \mathcal{W} \quad (61)$$

Each components is then related to  $L_b$ . Root carbon is set equal to leaf carbon, which is itself linear in LAI, and total stem carbon is related to  $L_b$  by a power law (Enquist et al., 1998):

$$\mathcal{L} = \sigma_l L_b \quad (62)$$

$$\mathcal{R} = \mathcal{L} \quad (63)$$

$$\mathcal{W} = a_{wl} L_b^{5/3} \quad (64)$$

Here  $\sigma_l$  is the specific leaf carbon density ( $\text{kg C m}^{-2}$  per unit of LAI) of the vegetation type, and  $a_{wl}$  is a PFT-dependent parameter.

Values of canopy height,  $h$ , are found directly from  $\mathcal{W}$  as described in Sect. 6.2.

The local litterfall rate,  $\Lambda_l$ , in Eq. (57), consists of contributions from leaf, root and stem carbon:

$$\Lambda_l = \gamma_l \mathcal{L} + \gamma_r \mathcal{R} + \gamma_w \mathcal{W} \quad (65)$$

where  $\gamma_l$ ,  $\gamma_r$  and  $\gamma_w$  are turnover rates ( $\text{yr}^{-1}$ ) for leaf, root and stem carbon respectively. The leaf turnover rate is calculated to be consistent with the phenological module as

**JULES: carbon fluxes and vegetation**

D. B. Clark et al.

Title Page

Abstract

Introduction

Conclusions

References

Tables

Figures

◀

▶

◀

▶

Back

Close

Full Screen / Esc

Printer-friendly Version

Interactive Discussion



described in Sect. 4. There is an additional litter contribution arising from large-scale disturbance which results in loss of vegetated area at the prescribed rate  $\gamma_v$ , as represented by the last term on the right-hand side of Eq. (58).

## 6.2 Updating of biophysical parameters

5 The land-surface parameters required by JULES are recalculated directly from the LAI and canopy height of each PFT, each time the vegetation cover is updated. Values of canopy height,  $h$ , are derived by assuming a fixed ratio,  $a_{ws}$ , of total stem carbon to respiring stem carbon:

$$\mathcal{W} = a_{ws} \mathcal{S} \quad (66)$$

10 where we assume  $a_{ws} = 10.0$  for woody plants and  $a_{ws} = 1.0$  for grasses (Friend et al., 1993, and Table 7). Combining with Eqs. (64) and (39) enables canopy height to be diagnosed directly from the total stem biomass:

$$h = \frac{\mathcal{W}}{a_{ws} \eta_{sl}} \left\{ \frac{a_{wl}}{\mathcal{W}} \right\}^{1/b_{wl}} \quad (67)$$

15 Given the canopy height and LAI, the values of biophysical parameters are calculated as described in Part 1.

## 6.3 Spin-up methodology

20 Soil carbon and vegetation fractions have timescales of order 100s–1000s years to reach equilibrium which would necessitate very long spin-up simulations. Hence, TRIFFID was designed to be used in both an “equilibrium” and a “dynamic” mode. The TRIFFID equations to update the plant fractional coverage and leaf area index are written to enable both explicit and implicit timestepping so that their discretisation can be reduced to the Newton-Raphson algorithm for iteratively approaching an equilibrium given external driving conditions. In equilibrium mode TRIFFID is coupled asynchronously to

Title Page

Abstract

Introduction

Conclusions

References

Tables

Figures

◀

▶

◀

▶

Back

Close

Full Screen / Esc

Printer-friendly Version

Interactive Discussion



**JULES: carbon fluxes  
and vegetation**

D. B. Clark et al.

[Title Page](#)[Abstract](#)[Introduction](#)[Conclusions](#)[References](#)[Tables](#)[Figures](#)[⏪](#)[⏩](#)[◀](#)[▶](#)[Back](#)[Close](#)[Full Screen / Esc](#)[Printer-friendly Version](#)[Interactive Discussion](#)

the rest of the model, with accumulated carbon fluxes passed from the physiology component after an integer number of years, typically every 5 years in order to smooth the effect of interannual variability. If JULES is being run with a single repeating year of meteorology then an equilibrium timestep of 1 year is sufficient. On each TRIFFID call, the vegetation and soil variables are updated iteratively using an implicit scheme with a long internal timestep. This approach is very effective in producing equilibrium states for the slowest variables (e.g. large soil carbon pools or forest cover).

Figure 3 shows the evolution of annual NPP and broad-leaf tree fraction when run in equilibrium mode for a single point, with annually repeating meteorology, from arbitrary initial conditions of 0, 35% and 100% broadleaf tree cover. Although the “real” timescale of tree growth would be decades to centuries, the spin-up mode converges to a steady state after just 5 calls to TRIFFID. In a global simulation this rapid equilibration technique is invaluable.

This implicit equilibrium mode has also been implemented for the 4-pool soil carbon model in JULES (Sect. 5.1), but a drawback is that sub-annual timescales which are important to the small, fast DPM pool are not captured by the multi-year equilibrium approach. The mean DPM implied by a seasonally-varying input of fluxes is not the same as the DPM implied by the annual mean of those fluxes. Hence, the equilibrium mode in JULES produces only an approximation of a steady soil-carbon state. To achieve a full spin-up, either JULES can subsequently be run in dynamic mode until steady state is reached, or the soil carbon model can be run offline from the rest of JULES using carbon fluxes and rate-modifiers as inputs.

## 7 Summary

JULES is based on the MOSES land surface scheme (Cox et al., 1999) and the TRIFFID dynamic global vegetation model (Cox, 2001), but with significant improvements. JULES includes several options for scaling photosynthesis from leaf to canopy scale, with the most complex modelling the profile of light interception through the vegetation

**JULES: carbon fluxes  
and vegetation**

D. B. Clark et al.

Title Page

Abstract

Introduction

Conclusions

References

Tables

Figures

◀

▶

◀

▶

Back

Close

Full Screen / Esc

Printer-friendly Version

Interactive Discussion



with a multi-layer scheme including representation of sunfleck penetration. The coupled model of leaf photosynthesis and stomatal conductance includes representation of the effect of ozone. Soil carbon processes are modelled using a 4-pool description and methane emissions from wetlands are also modelled. The performance of JULES is quantified using a system described by Blyth et al. (2010) which includes measures of land-atmosphere fluxes of CO<sub>2</sub>.

The inclusion of land-atmosphere exchanges of CO<sub>2</sub>, H<sub>2</sub>O, CH<sub>4</sub> and O<sub>3</sub> and aerosol effects in a single model framework is a significant development towards a comprehensive trace-gas enabled land surface model (Arneth et al., 2010). The development of JULES is ongoing, with revised or new representations of several key Earth system processes under consideration. These include a vegetation model based on a statistical approximation of a canopy gap model (Fisher et al., 2010b), a model of fire disturbance based on Thonicke et al. (2010), soil C and N cycles (Smith et al., 2007) coupled to a description of plant N uptake (Fisher et al., 2010a), and a model of biogenic isoprene emission (Pacifico et al., 2010). JULES will also be coupled to the IMOGEN system (Huntingford et al., 2010), thereby allowing a first-order assessment of how the biogeochemical processes represented in JULES might respond to, and in turn feed back on, a changing climate.

For further details of JULES, including how to acquire a copy of the code, see <http://www.jchmr.org/jules>.

*Acknowledgements.* C. Jones, N. Gedney, M. Best, M. Pryor and O. Boucher were supported by the Joint DECC/Defra Met Office Hadley Centre Climate Programme (GA01101).

**References**

Arneth, A., Sitch, S., Bondeau, A., Butterbach-Bahl, K., Foster, P., Gedney, N., de Noblet-Ducoudré, N., Prentice, I. C., Sanderson, M., Thonicke, K., Wania, R., and Zaehle, S.: From biota to chemistry and climate: towards a comprehensive description of trace gas exchange

**JULES: carbon fluxes  
and vegetation**

D. B. Clark et al.

[Title Page](#)[Abstract](#)[Introduction](#)[Conclusions](#)[References](#)[Tables](#)[Figures](#)[◀](#)[▶](#)[◀](#)[▶](#)[Back](#)[Close](#)[Full Screen / Esc](#)[Printer-friendly Version](#)[Interactive Discussion](#)

- between the biosphere and atmosphere, *Biogeosciences*, 7, 121–149, doi:10.5194/bg-7-121-2010, 2010. 643, 670
- Ashmore, M. R.: Assessing the future global impacts of ozone on vegetation, *Plant Cell Environ.*, 28, 949–964, 2005. 657
- 5 Atkin, O. K., Evans, J. R., and Siebke, K.: Relationship between the inhibition of leaf respiration by light and enhancement of leaf dark respiration following light treatment, *Aust. J. Plant Physiol.*, 25, 437–443, 1998. 655
- Atkin, O. K., Evans, J. R., Ball, M. C., Lambers, H., and Pons, T. L.: Leaf respiration of snow gum in the light and dark interactions between temperature and irradiance, *Plant Physiol.*, 122, 915–923, 2000. 655
- 10 Ball, J. T., Woodrow, I. E., and Berry, J. A.: A model predicting stomatal conductance and its contribution to the control of photosynthesis under different environmental conditions, in: *Progress in photosynthesis research*, edited by: Biggins, I., Martinus Nijhoff, Netherlands, 221–224, 1987. 649
- 15 Best, M. J., Pryor, M., Clark, D. B., Rooney, G. G., Essery, R. L. H., Ménard, C. B., Edwards, J. M., Hendry, M. A., Porson, A., Gedney, N., Mercado, L. M., Sitch, S., Blyth, E., Boucher, O., Cox, P. M., Grimmond, C. S. B., and Harding, R. J.: The Joint UK Land Environment Simulator (JULES), Model description – Part 1: Energy and water fluxes, *Geosci. Model Dev. Discuss.*, 4, 595–640, doi:10.5194/gmdd-4-595-2011, 2011. 645
- 20 Betts, R. A., Cox, P. M., Collins, M., Harris, P. P., Huntingford, C., and Jones, C. D.: The role of ecosystem-atmosphere interactions in simulated Amazonian precipitation decrease and forest dieback under global climate warming, *Theor. Appl. Climatol.*, 78, 157–175, 2004. 643
- Blyth, E., Clark, D. B., Ellis, R., Huntingford, C., Los, S., Pryor, M., Best, M., and Sitch, S.: A comprehensive set of benchmark tests for a land surface model of simultaneous fluxes of water and carbon at both the global and seasonal scale, *Geosci. Model Dev. Discuss.*, 3, 1829–1859, doi:10.5194/gmdd-3-1829-2010, 2010. 645, 655, 670
- 25 Brooks, A. and Farquhar, G. D.: Effect of temperature on the  $\text{CO}_2/\text{O}_2$  specificity of ribulose 1,5-bisphosphate carboxylase oxygenase and the rate of respiration in the light: estimates from gas exchange measurements on spinach., *Planta*, 165, 397–406, 1985. 654, 655
- 30 Cadule, P., Friedlingstein, P., Bopp, L., Sitch, S., Jones, C. D., Ciais, P., Piao, S. L., and Peylin, P.: Benchmarking coupled climate-carbon models against long-term atmospheric  $\text{CO}_2$  measurements, *Global Biogeochem. Cy.*, 24, GB2016, 10.1029/2009GB003556, 2010. 644
- Carswell, F. E., Meir, P., Wandelli, E. V., Bonates, L. C. M. and Kruijt, B., Barbosa, E. M., Nobre,

**JULES: carbon fluxes  
and vegetation**

D. B. Clark et al.

[Title Page](#)[Abstract](#)[Introduction](#)[Conclusions](#)[References](#)[Tables](#)[Figures](#)[◀](#)[▶](#)[◀](#)[▶](#)[Back](#)[Close](#)[Full Screen / Esc](#)[Printer-friendly Version](#)[Interactive Discussion](#)

- A. D., Grace, J., and Jarvis, P. G.: Photosynthetic capacity in a central Amazonian rain forest, *Planta*, 20, 179–186, 2000. 654
- Ciais, P., Tans, P. P., Trolier, M., White, J. W. C., and Francey, R. J.: A large northern hemisphere terrestrial CO<sub>2</sub> sink indicated by the <sup>13</sup>C/<sup>12</sup>C ratio of atmospheric CO<sub>2</sub>, *Science*, 269, 1098–1102, 1995. 642
- 5 Coleman, K. and Jenkinson, D. S.: RothC-26.3, a model for the turnover of carbon in soil: model description and user's guide, Tech. Rep., Lawes Agricultural Trust, Harpenden, UK, 1999. 644, 662
- Collatz, G. J., Ball, J. T., Grivet, C., and Berry, J. A.: Physiological and environmental regulation of stomatal conductance, photosynthesis and transpiration: a model that includes a laminar boundary layer, *Agr. Forest Meteorol.*, 54, 107–136, 1991. 647, 648
- 10 Collatz, G. J., Ribas-Carbo, M., and Berry, J. A.: Coupled photosynthesis-stomatal conductance model for leaves of C<sub>4</sub> plants, *Aust. J. Plant Physiol.*, 19, 519–538, 1992. 647, 648
- Cox, P. M.: Description of the TRIFFID Dynamic Global Vegetation Model, Hadley Centre Technical Note 24, Hadley Centre, Met Office, Bracknell, UK, 2001. 643, 646, 654, 659, 661, 663, 665, 669
- 15 Cox, P. M., Huntingford, C., and Harding, R. J.: A canopy conductance and photosynthesis model for use in a GCM land surface scheme, *J. Hydrol.*, 213, 79–94, 1998. 649
- Cox, P. M., Betts, R. A., Bunton, C. B., Essery, R. L. H., Rowntree, P. R., and Smith, J.: The impact of new land surface physics on the GCM simulation of climate and climate sensitivity, *Clim. Dynam.*, 15, 183–203, 1999. 643, 645, 646, 647, 649, 650, 657, 658, 669
- 20 Cox, P. M., Betts, R. A., Jones, C. D., Spall, S. A., and Totterdell, I. J.: Acceleration of global warming due to carbon-cycle feedbacks in a coupled climate model, *Nature*, 408, 184–187, 2000. 643
- 25 Cox, P. M., Betts, R. A., Collins, M., Harris, P. P., Huntingford, C., and Jones, C. D.: Amazonian forest dieback under climate-carbon cycle projections for the 21st Century, *Theor. Appl. Climatol.*, 78, 137–156, 2004. 643
- Cramer, W., Bondeau, A., Woodward, F. I., Prentice, I. C., Betts, R. A., Brovkin, V., Cox, P. M., Fisher, V., Foley, J. A., Friend, A. D., Kucharik, C., Lomas, M. R., Ramankutty, N., Sitch, S., Smith, B., White, A., and Young-Molling, C.: Global response of terrestrial ecosystem structure and function to CO<sub>2</sub> and climate change: Results from six dynamic global vegetation models, *Global Change Biol.*, 7, 357–374, 2001. 643
- 30 Dai, Y. J., Dickinson, R. E., and Wang, Y. P.: A two-big-leaf model for canopy temperature,

photosynthesis, and stomatal conductance, *J. Climate*, 17, 2281–2299, 2004. 652

de Pury, D. G. G. and Farquhar, G. D.: Simple scaling of photosynthesis from leaves to canopies without the errors of big-leaf, *Plant Cell Environ.*, 20, 537–557, 1997. 654

Enquist, B., Brown, J., and West, G.: Allometric scaling of plant energetics and population density, *Nature*, 395, 163–166, 1998. 667

Essery, R., Best, M., and Cox, P.: MOSES 2.2 Technical Documentation, Hadley Centre Technical Note 30, Hadley Centre, Met Office, Bracknell, UK, 2001. 651

Essery, R. L. H., Best, M. J., Betts, R. A., Cox, P. M., and Taylor, C. M.: Explicit representation of subgrid heterogeneity in a GCM land surface scheme, *J. Hydrometeorol.*, 4, 530–543, 2003. 643

Fisher, J. B., Sitch, S., Malhi, Y., Fisher, R. A., Huntingford, C., and Tan, S.-Y.: Carbon cost of plant nitrogen acquisition: A mechanistic, globally applicable model of plant nitrogen uptake, retranslocation, and fixation, *Global Biogeochem. Cy.*, 24, doi:10.1029/2009GB003621, 2010a. 670

Fisher, R., McDowell, N., Purves, D., Moorcroft, P., Sitch, S., Cox, P., Huntingford, C., Meir, P., and Woodward, F. I.: Assessing uncertainties in a second-generation dynamic vegetation model caused by ecological scale limitations, *New Phytol.*, 187, 666–681, doi:10.1111/j.1469-8137.2010.03340.x, 2010b. 670

Friedlingstein, P., Cox, P. M., Betts, R. A., Bopp, L., von Bloh, W., Brovkin, V., Cadule, P., Doney, S., Eby, M., Fung, I., Bala, G., John, J., Jones, C. D., Joos, F., Kato, T., Kawamiya, M., Knorr, W., Lindsay, K., Matthews, H. D., Raddatz, T., Rayner, P., Reick, C., Roeckner, E., Schnitzler, K. G., Schnur, R., Strassmann, K., Weaver, A. J., Yoshikawa, C., and Zeng, N.: Climate–carbon cycle feedback analysis, results from the C4MIP model intercomparison, *J. Climate*, 19, 3337–3353, doi:10.1175/JCLI3800.1, 2006. 643

Friend, A. D., Shugart, H. H., and Running, S. W.: A physiology-based model of forest dynamics, *Ecology*, 74, 792–797, 1993. 659, 668

Gedney, N., Cox, P. M., and Huntingford, C.: Climate feedback from wetland methane emissions, *Geophys. Res. Lett.*, 31, L20503, doi:10.1029/2004GL020919, 2004. 644, 664

Hoefnagel, M. H. N., Atkin, O. K., and Wiskich, J. T.: Interdependence between chloroplasts and mitochondria in the light and the dark, *Bba-Bioenergetics*, 1366, 235–255, 1998. 655

Huntingford, C., Booth, B. B. B., Sitch, S., Gedney, N., Lowe, J. A., Liddicoat, S. K., Mercado, L. M., Best, M. J., Weedon, G. P., Fisher, R. A., Lomas, M. R., Good, P., Zelazowski, P., Everitt, A. C., Spessa, A. C., and Jones, C. D.: IMOGEN: an intermediate complexity

**GMDD**

4, 641–688, 2011

---

**JULES: carbon fluxes  
and vegetation**

D. B. Clark et al.

---

[Title Page](#)

[Abstract](#)

[Introduction](#)

[Conclusions](#)

[References](#)

[Tables](#)

[Figures](#)

[◀](#)

[▶](#)

[◀](#)

[▶](#)

[Back](#)

[Close](#)

[Full Screen / Esc](#)

[Printer-friendly Version](#)

[Interactive Discussion](#)



**JULES: carbon fluxes  
and vegetation**

D. B. Clark et al.

[Title Page](#)[Abstract](#)[Introduction](#)[Conclusions](#)[References](#)[Tables](#)[Figures](#)[◀](#)[▶](#)[◀](#)[▶](#)[Back](#)[Close](#)[Full Screen / Esc](#)[Printer-friendly Version](#)[Interactive Discussion](#)

model to evaluate terrestrial impacts of a changing climate, *Geosci. Model Dev.*, 3, 679–687, doi:10.5194/gmd-3-679-2010, 2010. 670

Jacobs, C.: Direct impact of atmospheric CO<sub>2</sub> enrichment on regional transpiration, Ph.D. thesis, Wageningen Agricultural University, 1994. 649

5 Jenkinson, D. S.: The turnover of organic-carbon and nitrogen in soil, *Philos. T. R. Soc. Lond.*, 329, 361–368, 1990. 644, 662, 687

Jogireddy, V., Cox, P. M., Huntingford, C., Harding, R. J., and M., M. L.: An improved description of canopy light interception for use in a GCM land-surface scheme: calibration and testing against carbon fluxes at a coniferous forest, Hadley Centre Technical Note 63, Hadley Centre, Met Office, Exeter, UK, 2006. 652, 655

10 Jones, C. D. and Falloon, P. D.: Sources of uncertainty in global modelling of future soil organic carbon storage, in: *Uncertainties in Environmental Modelling and Consequences for Policy Making*. NATO Science for Peace and Security Series, edited by: Baveye, P., Mysiak, J., and Laba, M., Springer, Dordrecht, Netherlands, 283–315, 2009. 663

15 Jones, C. D., Cox, P. M., Essery, R. L. H., Roberts, D. L., and Woodage, M. J.: Strong carbon cycle feedbacks in a climate model with interactive CO<sub>2</sub> and sulphate aerosols, *Geophys. Res. Lett.*, 30, doi:10.1029/2003GL016867, 2003. 644

Jones, C. D., McConnell, C., Coleman, K. W., Cox, P., Falloon, P. D., Jenkinson, D., and Powlson, D.: Global climate change and soil carbon stocks; predictions from two contrasting models for the turnover of organic carbon in soil, *Glob. Change Biol.*, 11, 154–166, doi:10.1111/j.1365-2486.2004.00885.x, 2005. 644, 664

20 Jones, C. D., Cox, P. M., and Huntingford, C.: Climate-carbon cycle feedbacks under stabilization, *Tellus A*, 58B, doi:10.1111/j.1600-0889.2006.00217.x, 2006. 643

Karlsson, P. E., Uddling, J., Braun, S., Broadmeadow, M., Elvira, S., Gimeno, B. S., Le Thiec, D., Oksanen, E., Vandermeiren, K., Wilkinson, M., and Emberson, L.: New critical levels for ozone effects on young trees based on AOT40 and simulated cumulative leaf uptake of ozone, *Atmos. Environ.*, 38, 2283–2294, 2004. 658

25 Knohl, A., Schulze, E. D., Kolle, O., and Buchmann, N.: Large carbon uptake by an unmanaged 250-year-old deciduous forest in Central Germany, *Agr. Forest Meteorol.*, 118, 151–167, 2003. 656

30 Le Quéré, C., Raupach, M. R., Canadell, J. G., Marland, G., Bopp, L., Ciais, P., Conway, T. J., Doney, S. C., Feely, R. A., Foster, P., Friedlingstein, P., Gurney, K., Houghton, R. A., House, J. I., Huntingford, C., Levy, P. E., Lomas, M. R., Majkut, J., Metzl, N., Ometto, J. P., Peters,

**JULES: carbon fluxes  
and vegetation**

D. B. Clark et al.

[Title Page](#)[Abstract](#)[Introduction](#)[Conclusions](#)[References](#)[Tables](#)[Figures](#)[◀](#)[▶](#)[◀](#)[▶](#)[Back](#)[Close](#)[Full Screen / Esc](#)[Printer-friendly Version](#)[Interactive Discussion](#)

G. P., Prentice, I. C., Randerson, J. T., Running, S. W., Sarmiento, J. L., Schuster, U., Sitch, S., Takahashi, T., Viovy, N., van der Werf, G. R., and Woodward, F. I.: Trends in the sources and sinks of carbon dioxide, *Nature Geosci.*, 2, 831–836, 2009. 642

Leuning, R.: A critical appraisal of a combined stomatal-photosynthesis model for  $C_3$  plants, *Plant Cell Environ.*, 18, 357–364, 1995. 649

Lloyd, J., Grace, J., Miranda, A. C., Meir, P., Wong, S. C., Miranda, B. S., Wright, I. R., Gash, J. H. C., and McIntyre, J.: A Simple Calibrated Model of Amazon Rain-Forest Productivity Based on Leaf Biochemical-Properties, *Plant, Cell Environ.*, 18, 1129–1145, 1995. 654

McGuire, A. D., Sitch, S. A., Clein, J. S., Dargaville, R., Esser, G., Foley, J., Heimann, M., Joos, F., Kaplan, J. O., Kicklighter, D. W., Meier, R. A., Moore-III, B., Prentice, I. C., Ramankutty, N., Reichenau, T., Schloss, A., Tian, H., Williams, L. J., and Wittenberg, U.: Carbon Balance of the Terrestrial Biosphere in the Twentieth Century: Analyses of  $CO_2$ , Climate and Land Use Effects With Four Process-Based Ecosystem Models, *Global Biogeochem. Cy.*, 15, 183–206, 2001. 642

Meir, P., Kruijt, B., Broadmeadow, M., Barbosa, E., Kull, O., Carswell, F., Nobre, A., and Jarvis, P. G.: Acclimation of photosynthetic capacity to irradiance in tree canopies in relation to leaf nitrogen concentration and leaf mass per unit area, *Plant Cell Environ.*, 25, 343–357, 2002. 655

Mercado, L. M., Huntingford, C., Gash, J. H. C., Cox, P. M., and Jogireddy, V.: Improving the representation of radiation interception and photosynthesis for climate model applications, *Tellus B*, 59, 553–565, 2007. 654, 655

Mercado, L. M., Bellouin, N., Sitch, S., Boucher, O., Huntingford, C., M., W., and Cox, P. M.: Impact of Changes in Diffuse Radiation on the Global Land Carbon Sink, *Nature*, 458, 1014–1018, 2009. 644, 652, 656

Monsi, M. and Saeki, T.: Ueber den Lichtfaktor in den Pflanzengesellschaften und seine Bedeutung fuer die Stoffproduktion, *Jap. J. Bot.*, 14, 22–52, 1953. 650

Pacifico, F., Harrison, S. P., Jones, C. D., Arneeth, A., Sitch, S., Weedon, G. P., Barkley, M. P., Palmer, P. I., Serça, D., Potosnak, M., Fu, T. M., Goldstein, A., Bai, J., and Schurgers, G.: Evaluation of a photosynthesis-based biogenic isoprene emission scheme in JULES and simulation of isoprene emissions under modern climate conditions, *Atmos. Chem. Phys. Discuss.*, 10, 28311–28354, doi:10.5194/acpd-10-28311-2010, 2010. 670

Phillips, O. L., Aragao, L. E. O. C., Lewis, S. L., Fisher, J. B., Lloyd, J., Lopez-Gonzalez, G., Malhi, Y., Monteagudo, A., Peacock, J., Quesada, C. A., van der Heijden, G., Almeida, S.,

**JULES: carbon fluxes  
and vegetation**

D. B. Clark et al.

[Title Page](#)[Abstract](#)[Introduction](#)[Conclusions](#)[References](#)[Tables](#)[Figures](#)[◀](#)[▶](#)[◀](#)[▶](#)[Back](#)[Close](#)[Full Screen / Esc](#)[Printer-friendly Version](#)[Interactive Discussion](#)

Amaral, I., Arroyo, L., Aymard, G., Baker, T. R., Banki, O., Blanc, L., Bonal, D., Brando, P.,  
Chave, J., Alves de Oliveira, A. C., Cardozo, N. D., Czimczik, C. I., Feldpausch, T. R., Freitas,  
M. A., Gloor, E., Higuchi, N., Jimenez, E., Lloyd, G., Meir, P., Mendoza, C., Morel, A., Neill,  
D. A., Nepstad, D., Patino, S., Cristina Penuela, M., Prieto, A., Ramirez, F., Schwarz, M.,  
5 Silva, J., Silveira, M., Thomas, A. S., ter Steege, H., Stropp, J., Vasquez, R., Zelazowski,  
P., Alvarez Davila, E., Andelman, S., Andrade, A., Chao, K.-J., Erwin, T., Di Fiore, A., Hon-  
orio C, E., Keeling, H., Killeen, T. J., Laurance, W. F., Pena Cruz, A., Pitman, N. C. A.,  
Nunez Vargas, P., Ramirez-Angulo, H., Rudas, A., Salamao, R., Silva, N., Terborgh, J., and  
Torres-Lezama, A.: Drought sensitivity of the Amazon rainforest, *Science*, 323, 1344–1347,  
10 doi:10.1126/science.1164033, 2009. 642

Pleijel, H., Danielsson, H., Ojanperä, K., De Temmerman, L., Högy, P., Badiani, M., and Karls-  
son, P. E.: Relationships between ozone exposure and yield loss in European wheat and  
potato- a comparison of concentration- and flux-based exposure indices, *Atmos. Environ.*,  
38, 2259–2269, 2004. 657, 658

15 Prentice, I. C., Farquhar, G. D., Fasham, M. J. R., Goulden, M. L., Heimann, M., Jaramillo,  
V. J., Kheshgi, H. S., Le Quéré, C., Scholes, R. J., and Wallace, D. W. R.: Dynamic Global  
Vegetation Modeling: Quantifying Terrestrial Ecosystem Responses to Large-Scale Environ-  
mental Change, in: *Climate Change 2001: The Scientific Basis. Contribution of Working  
Group I to the Third Assessment Report of the Intergovernmental Panel on Climate Change*,  
20 edited by Houghton, J. T., Ding, Y., Griggs, D. J., Noguer, M., van der Linden, P. J., Dai, X.,  
Maskell, K., and Johnson, C. A., Cambridge University Press, Cambridge, United Kingdom  
and New York, NY, USA, 183–237, 2001. 642

Prentice, I. C., Bondeau, A., Cramer, W., Harrison, S. P., Hickler, T., Lucht, W., Sitch, S., Smith,  
B., and Sykes, M. T.: Dynamic global vegetation modeling: quantifying terrestrial ecosystem  
25 responses to large-scale environmental change, in: *Terrestrial Ecosystems in a Changing  
World*, edited by: Canadell, J., Pitelka, L., and Pataki, D., IGBP Book Series, Springer,  
Heidelberg, Germany, 175–192, 2007. 643

Rebmann, C., Zeri, M., Lasslop, G., Kolle, O., Schulze, E. D., and Feigenwinter, C.: Treatment  
and assessment of the CO<sub>2</sub>-exchange at a complex forest site in Thuringia, Germany, *Agr.  
Forest Meteorol.*, 150, 684–691, 2010. 656

30 Sellers, P., Randall, D., Collatz, C., Berry, J., Field, C., Dazlich, D., Zhang, C., and Collelo,  
G.: A revised land surface parameterisation (SiB2) for atmospheric GCMs. Part I: Model  
formulation, *J. Climate*, 9, 676–705, 1996. 647

- Sellers, P. J.: Canopy Reflectance, Photosynthesis, and Transpiration III. A Reanalysis Using Improved Leaf Models and a New Canopy Integration Scheme, *Int. J. Remote Sens.*, 6, 1335–1372, 1985. 651, 655
- Sellers, P. J., Berry, J. A., Collatz, G. J., Field, C. B., and Hall, F. G.: Canopy Reflectance, Photosynthesis, and Transpiration III. A Reanalysis Using Improved Leaf Models and a New Canopy Integration Scheme, *Remote Sens. Environ.*, 42, 187–216, 1992. 650
- Shulze, E. D., Kelliher, F. M., Korner, C., and Lloyd, J.: Relationships among maximum stomatal conductance, ecosystem surface conductance, carbon assimilation rate, and plant nitrogen nutrition: a global ecology scaling exercise, *Annu. Rev. Ecol. Sys.*, 25, 629–660, 1994. 654
- Sitch, S., Smith, B., Prentice, I. C., Arneth, A., Bondeau, A., Cramer, W., Kaplan, J. O., Levis, S., Lucht, W., Sykes, M. T., Thonicke, K., and Venevsky, S.: Evaluation of ecosystem dynamics, plant geography and terrestrial carbon cycling in the LPJ dynamic global vegetation model, *Glob. Change Biol.*, 9, 161–185, 2003. 643
- Sitch, S., Cox, P. M., Collins, W. J., and Huntingford, C.: Indirect radiative forcing of climate change through ozone effects on the land-carbon sink, *Nature*, 448, 791–794, 2007. 644, 657, 658, 681
- Sitch, S., Huntingford, C., Gedney, N., Levy, P. E., Lomas, M., Piao, S. L., Betts, R. A., Ciais, P., Cox, P. M., Friedlingstein, P., Jones, C. D., Prentice, I. C., and Woodward, F. I.: Evaluation of the terrestrial carbon cycle, future plant geography and climate-carbon cycle feedbacks using five Dynamic Global Vegetation Models (DGVMs), *Global Change Biol.*, 14, 2015–2039, doi:10.1111/j.1365-2486.2008.01626.x, 2008. 643
- Smith, P., Smith, J. U., Flynn, H., Killham, K., Rangel-Castro, I., Foereid, B., Aitkenhead, M., Chapman, S., Towers, W., Bell, J., Lumsdon, D., Milne, R., Thomson, A., Simmons, I., Skiba, U., Reynolds, B., Evans, C., Frogbrook, Z., Bradley, I., Whitmore, A., and Falloon, P.: ECOSSE: Estimating Carbon in Organic Soils - Sequestration and Emissions. Final Report., Tech. rep., SEERAD, <http://www.scotland.gov.uk/Publications/2007/03/16170508/16>, last access: 21 February 2011, 2007. 670
- Sokolov, A., Kicklighter, D., Melillo, J., Felzer, B., Schlosser, C., and Cronin, T.: Consequences of considering carbon-nitrogen interactions on the feedbacks between climate and the terrestrial carbon cycle, *J. Climate*, 21, 3776–3796, doi:10.1175/2008JCLI2038.1, 2008. 643
- Stephens, B. B., Gurney, K. R., Tans, P. P., Sweeney, C., Peters, W., Bruhwiler, L., Ciais, P., Ramonet, M., Bousquet, P., Nakazawa, T., Aoki, S., Machida, T., Inoue, G., Vinnichenko, N., Lloyd, J., Jordan, A., Heimann, M., Shibistova, O., Langenfelds, R. L., Steele, L. P., Francey,

**GMDD**

4, 641–688, 2011

---

**JULES: carbon fluxes  
and vegetation**

D. B. Clark et al.

---

Title Page

Abstract

Introduction

Conclusions

References

Tables

Figures

◀

▶

◀

▶

Back

Close

Full Screen / Esc

Printer-friendly Version

Interactive Discussion



R. J., and Denning, A. S.: Weak northern and strong tropical land carbon uptake from vertical profiles of atmospheric CO<sub>2</sub>, *Science*, 316, 1732–1735, doi:10.1126/science.1137004, 2007. 642

Thonicke, K., Spessa, A., Prentice, I. C., Harrison, S. P., Dong, L., and Carmona-Moreno, C.: The influence of vegetation, fire spread and fire behaviour on biomass burning and trace gas emissions: results from a process-based model, *Biogeosciences*, 7, 1991–2011, doi:10.5194/bg-7-1991-2010, 2010. 670

Thornton, P. E., Lamarque, J. F., Rosenbloom, N., and Mahowald, N.: Influence of carbon-nitrogen cycle coupling on land model response to CO<sub>2</sub> fertilization and climate variability, *Global Biogeochem. Cy.*, 21, GB4018, doi:10.1029/2006GB002868, 2007. 643

**GMDD**

4, 641–688, 2011

---

**JULES: carbon fluxes  
and vegetation**

D. B. Clark et al.

---

Title Page

Abstract

Introduction

Conclusions

References

Tables

Figures

⏪

⏩

◀

▶

Back

Close

Full Screen / Esc

Printer-friendly Version

Interactive Discussion



## JULES: carbon fluxes and vegetation

D. B. Clark et al.

**Table 1.** Default values of PFT-specific parameters for leaf biochemistry and photosynthesis.

		Broadleaf tree	Needleleaf tree	C <sub>3</sub> grass	C <sub>4</sub> grass	Shrub
$k$	Extinction coefficient for PAR	0.50	0.50	0.50	0.50	0.50
$\alpha$ (mol CO <sub>2</sub> [mol PAR photons] <sup>-1</sup> )	Quantum efficiency	0.08	0.08	0.12	0.060	0.08
$\omega$	Leaf scattering coefficient for PAR	0.15	0.15	0.15	0.17	0.15
$f_d$	Dark respiration coefficient	0.015	0.015	0.015	0.025	0.015
$r_g$	Growth respiration coefficient	0.25	0.25	0.25	0.25	0.25
$N_0$ (kg N [kg C] <sup>-1</sup> )	Top leaf Nitrogen concentration	0.046	0.033	0.073	0.060	0.060
$n_{rl}$	Ratio of Nitrogen concentrations in roots and leaves	1.00	1.00	1.00	1.00	1.00
$n_{sl}$	Ratio of Nitrogen concentrations in stem and leaves	0.10	0.10	1.00	1.00	0.10
$T_{low}$ (°C)	Lower temperature parameter	0.0	-10.0	0.0	13.0	0.0
$T_{upp}$ (°C)	Upper temperature parameter	36.0	26.0	36.0	45.0	36.0

Title Page

Abstract

Introduction

Conclusions

References

Tables

Figures

◀

▶

◀

▶

Back

Close

Full Screen / Esc

Printer-friendly Version

Interactive Discussion



**JULES: carbon fluxes  
and vegetation**

D. B. Clark et al.

**Table 2.** Summary of options available for the calculation of canopy photosynthesis.

Option	Leaf to canopy scaling	Radiation	N profile	Inhibition of leaf respiration in light
1	Big leaf	Beer's law	Beer's law	no
2	Multi-layer	Two stream	Constant through canopy	no
3	Multi-layer radiation with two layers (sunlit and shaded) for photosynthesis	Two stream	Constant through canopy	no
4	Multi-layer	Two stream	Decreases through canopy	yes
5	Multi-layer including sunlit and shaded leaves in each layer	Two stream with sunfleck penetration	Decreases through canopy	yes

[Title Page](#)[Abstract](#)[Introduction](#)[Conclusions](#)[References](#)[Tables](#)[Figures](#)[I◀](#)[▶I](#)[◀](#)[▶](#)[Back](#)[Close](#)[Full Screen / Esc](#)[Printer-friendly Version](#)[Interactive Discussion](#)

**JULES: carbon fluxes  
and vegetation**

D. B. Clark et al.

[Title Page](#)[Abstract](#)[Introduction](#)[Conclusions](#)[References](#)[Tables](#)[Figures](#)[I◀](#)[▶I](#)[◀](#)[▶](#)[Back](#)[Close](#)[Full Screen / Esc](#)[Printer-friendly Version](#)[Interactive Discussion](#)**Table 3.** Default values of PFT-specific parameters for ozone effects. The values for  $a$  are the low sensitivity values from Sitch et al. (2007).

		Broadleaf tree	Needleleaf tree	C <sub>3</sub> grass	C <sub>4</sub> grass	Shrub
$F_{O_3 \text{ crit}}$ (nmol m <sup>-2</sup> s <sup>-1</sup> )	Threshold ozone flux	1.6	1.6	5.0	5.0	1.6
$a$ (mmol <sup>-1</sup> m <sup>-2</sup> )	Ozone factor	0.04	0.02	0.25	0.13	0.03

## JULES: carbon fluxes and vegetation

D. B. Clark et al.

**Table 4.** Default values of PFT-specific parameters for phenology.

		Broadleaf tree	Needleleaf tree	C <sub>3</sub> grass	C <sub>4</sub> grass	Shrub
$\gamma_0$ (360 days) <sup>-1</sup>	Minimum leaf turnover rate	0.25	0.25	0.25	0.25	0.25
$d_M$ (360 days) <sup>-1</sup>	Rate of change of turnover with soil moisture	0.0	0.0	0.0	0.0	0.0
$d_T$ (360 days K) <sup>-1</sup>	Rate of change of turnover with temperature	9.0	9.0	9.0	9.0	9.0
$M_{\text{off}}$	Threshold soil moisture	0.00	0.00	0.00	0.00	0.00
$T_{\text{off}}$ (K)	Threshold temperature	278.15	233.15	278.15	278.15	233.15
$\gamma_p$ (360 days) <sup>-1</sup>	Rate of leaf growth	15.00	20.00	20.00	20.00	20.00

Title Page

Abstract

Introduction

Conclusions

References

Tables

Figures

◀

▶

◀

▶

Back

Close

Full Screen / Esc

Printer-friendly Version

Interactive Discussion



**JULES: carbon fluxes  
and vegetation**

D. B. Clark et al.

[Title Page](#)[Abstract](#)[Introduction](#)[Conclusions](#)[References](#)[Tables](#)[Figures](#)[I◀](#)[▶I](#)[◀](#)[▶](#)[Back](#)[Close](#)[Full Screen / Esc](#)[Printer-friendly Version](#)[Interactive Discussion](#)**Table 5.** Default values of pool-specific parameters for soil carbon. The pools are decomposable and resistant plant material (DPM, RPM), biomass (BIO) and humus (HUM).

		DPM	RPM	BIO	HUM
$\kappa_s$ (s <sup>-1</sup> )	Soil specific respiration rate	$3.22 \times 10^{-7}$	$9.65 \times 10^{-9}$	$2.12 \times 10^{-8}$	$6.43 \times 10^{-10}$

**JULES: carbon fluxes  
and vegetation**

D. B. Clark et al.

**Table 6.** Default values of PFT-specific parameters for TRIFFID.

		Broadleaf tree	Needleleaf tree	C <sub>3</sub> grass	C <sub>4</sub> grass	Shrub
$\gamma_v$ (360 days) <sup>-1</sup>	Disturbance rate	0.005	0.007	0.20	0.20	0.05
$\gamma_r$ (360 days) <sup>-1</sup>	Turnover rate for root biomass	0.25	0.15	0.25	0.25	0.25
$\gamma_w$ (360 days) <sup>-1</sup>	Turnover rate for woody biomass	0.005	0.005	0.20	0.20	0.05
$L_{max}$	Maximum LAI	9.00	5.00	4.00	4.00	3.00
$L_{min}$	Minimum LAI	1.00	1.00	1.00	1.00	1.00

Title Page

Abstract

Introduction

Conclusions

References

Tables

Figures

I◀

▶I

◀

▶

Back

Close

Full Screen / Esc

Printer-friendly Version

Interactive Discussion





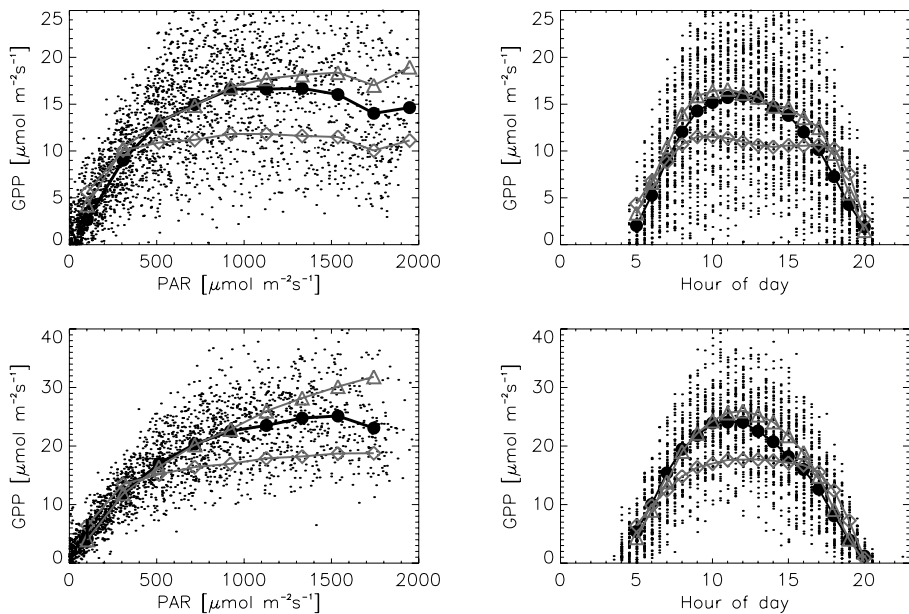


**Fig. 1.** Evaluation of modelled carbon uptake at a temperate broad leaf (top panel) and needle leaf site (bottom panel). Plots on the left represent the light response of Gross Primary Productivity (GPP) and on the right represent the diurnal cycle of GPP. Lines represent data (closed circles) and model simulations using the big leaf (open rhombus) and multi-layer approaches (open triangles). On the left, both data and simulations are averaged over 200 micromol quanta  $\text{m}^{-2} \text{s}^{-1}$  intervals, and on the right data and simulations are averaged over half hour time periods. In all cases dots represent half-hourly estimated GPP from eddy correlation.

Title Page

Abstract

Introduction

Conclusions

References

Tables

Figures



Back

Close

Full Screen / Esc

Printer-friendly Version

Interactive Discussion



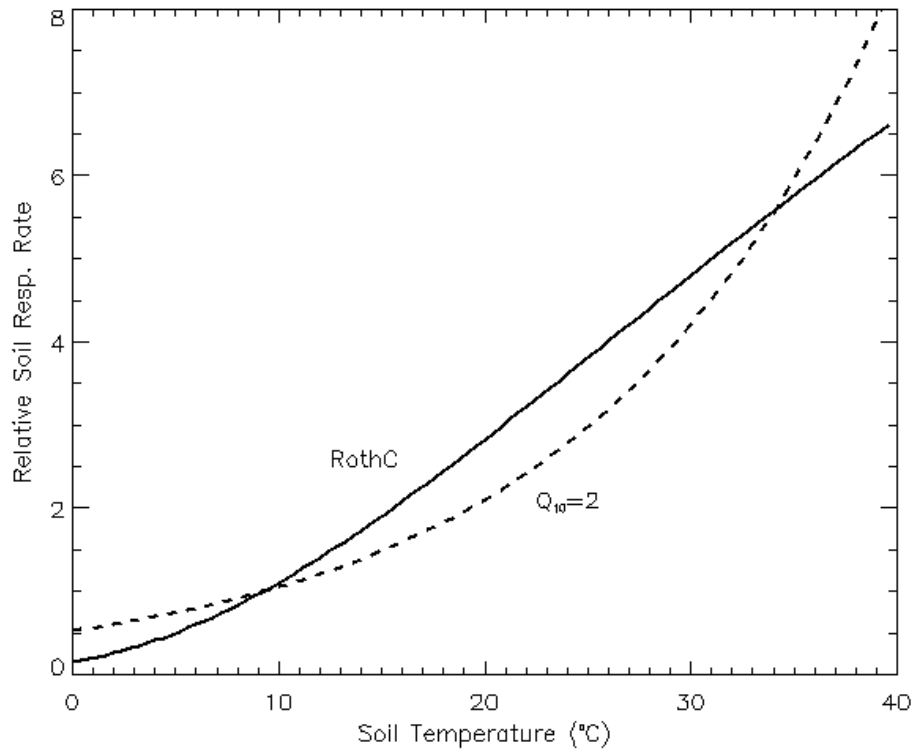


**Fig. 2.** Comparison of alternative forms for the sensitivity of specific soil respiration to soil temperature in JULES. The dashed line shows a  $Q_{10}$  form with  $Q_{10} = 2$ , the solid line shows the form from the RothC model (Jenkinson, 1990).

**JULES: carbon fluxes and vegetation**

D. B. Clark et al.

Title Page

Abstract

Introduction

Conclusions

References

Tables

Figures

◀

▶

◀

▶

Back

Close

Full Screen / Esc

Printer-friendly Version

Interactive Discussion



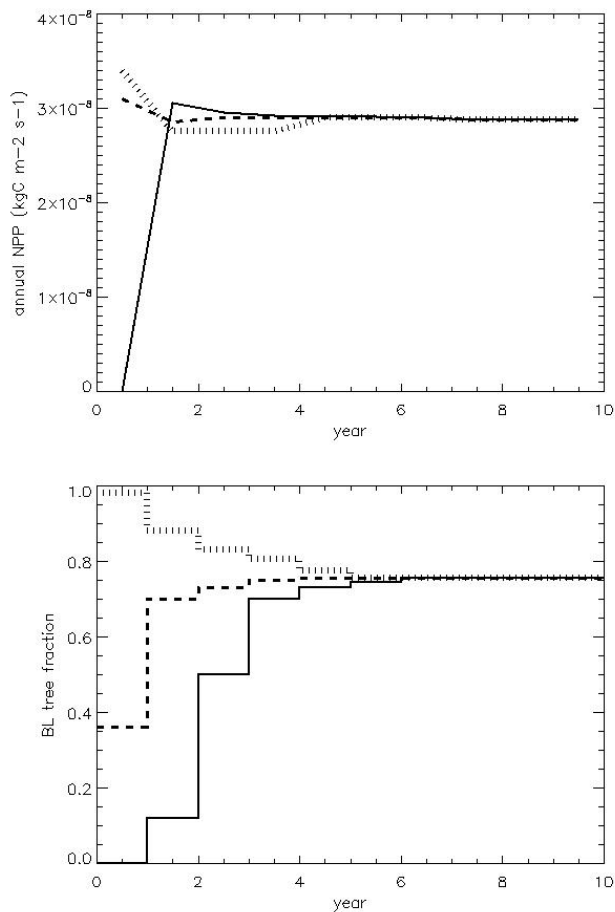


**Fig. 3.** An example of the spin up of TRIFFID in equilibrium mode. The lines show evolution from different initial conditions with convergence after five calls to TRIFFID. (Top) NPP (Bottom) the fractional coverage of the broadleaf tree type.

[Title Page](#)  
[Abstract](#)   [Introduction](#)  
[Conclusions](#)   [References](#)  
[Tables](#)   [Figures](#)  
[◀](#)   [▶](#)  
[◀](#)   [▶](#)  
[Back](#)   [Close](#)  
[Full Screen / Esc](#)  
[Printer-friendly Version](#)  
[Interactive Discussion](#)

